Band-Structure Effects on Itinerant-Electron Magnetism. II

S. ALEXANDER
Department of Nuclear Physics, Weizmann Institute of Science, Rehovoth, Israel
AND
G. HORWITZ*
Belfer Graduate School of Science, Yeshiva University, New York, New York

(Received 13 March 1967)

The magnetic properties of a simple nondegenerate band with short-range intra-atomic electron-electron interactions are discussed. A generalized Hartree-Fock formalism is developed which give closed expressions for all ordered magnetic states with constant local moments lying on a conical helix. The stability of the paramagnetic and ferromagnetic states with respect to these helixes is analyzed in detail. In particular, the importance of band structure and Fermi-surface geometry is investigated. It is shown that helical and antiferromagnetic magnetic states can indeed be more favorable than a ferromagnetic state for itinerant-band electrons with short-range interactions. It is shown that umklapp processes at the zone boundaries can favor antiferromagnetic instabilities of the paramagnetic state, and necks in the Fermi surface tend to favor spin-density waves with a period determined by the diameter of the neck. Related effects also appear in investigating the transverse stability of ferromagnetic states. Detailed numerical calculations on several simple model tight-binding band structures are presented to illustrate these arguments. The effects of the shape of the density-of-states curve and band ferromagnetism are also discussed, and conditions for discontinuities in the self-constent solutions are investigated.

I. INTRODUCTION

THERE are many reasons to believe that interatomic exchange is relatively unimportant in determining the magnetic behavior of metals. The arguments for this belief are partly physical and partly numerical, and have been discussed in great detail by Mott[1] and by Herring.[2]

The predominant electron-electron interactions responsible for magnetism are then intra-atomic Coulomb repulsions and exchange interactions, i.e., confined to the Wannier functions at each lattice site separately. As in insulators, these interactions give rise to a tendency to form local (ionic) magnetic moments. In a metal this tendency has to compete with the single-electron effects of the periodic potential. The over-all magnetic behavior of a metal is determined by a compromise between these two effects.

In insulators,[3] it was found possible to treat the effect of the single-electron periodic potential as a perturbation and calculate the effective magnetic interactions (e.g., superexchange) between local moments. In metals the situation is much more complicated. A large part of the conceptual difficulty in understanding the magnetic behavior of itinerant electrons results from the fact that the dominant electron-electron interactions are localized and are therefore best described in terms of the Wannier functions of the band, while the single-electron effects are only clear in a Bloch representation.

Consider, for example, the simplest situation, i.e., that of a nondegenerate band[4] on a Bravais lattice. There is then only one Wannier function per lattice site. The only localized interaction term is the local Coulomb interaction

$$H_{\rm int}=\sum_{\alpha} U n_{\alpha\uparrow} n_{\alpha\downarrow}, \tag{1}$$

where the summation is over all lattice sites (α), and

$$U=e^2 \int d\mathbf{r}_1 d\mathbf{r}_2 \mid w_\alpha(\mathbf{r}_1) \mid^2 \mid w_\alpha(\mathbf{r}_2) \mid^2 / \mid \mathbf{r}_1-\mathbf{r}_2 \mid, \tag{2}$$

with

$$n_{\alpha\sigma}=c_{\alpha\sigma}^{\dagger} c_{\alpha\sigma}, \tag{3}$$

the number operators for the occupation of the Wannier states $w_\alpha(\mathbf{r})$ having spin σ.

If one transforms to a Bloch representation (annihilation operator $c_{k\sigma}$),

$$c_{\alpha\sigma}=(1/\sqrt{N}) \sum_{\rm k} \exp(i\mathbf{k}\cdot\mathbf{r}_\alpha) c_{\rm k\sigma}, \tag{4}$$

one gets

$$H_{\rm int}=(U/N) \sum_{\rm k,k',l,l'} \delta(\mathbf{k}-\mathbf{k}'+\mathbf{l}-\mathbf{l}'-\mathbf{K}) c_{\rm k\uparrow}^{\dagger} c_{\rm k'\uparrow} c_{\rm l\downarrow}^{\dagger} c_{\rm l'\downarrow}, \tag{5}$$

where the summation is over the Brillouin zone and $\mathbf{K}$ is a reciprocal lattice vector. Equation (5) is, of course, quite complicated, and in addition to the diagonal Coulomb ($\mathbf{k}=\mathbf{k}'$, $\mathbf{l}=\mathbf{l}'$) and exchange ($\mathbf{k}=\mathbf{l}'$, $\mathbf{k}'=\mathbf{l}$) terms it contains more complex scattering terms. To retain the specifically local character of the interaction, Eq. (1) requires a detailed treatment of the scattering terms which can not be done by

* Supported by the U.S. Air Force Office of Scientific Research under Grant No. 508-66.

[1] N. F. Mott, Advan. Phys. **13**, 325 (1964).

[2] C. Herring, in *Exchange Interactions Among Itinerant Electrons in Magnetism*, edited by G. T. Rado and H. Suhl (Academic Press Inc., New York, 1963), Vol. 4.

[3] P. W. Anderson, in *Exchange Interactions Among Itinerant Electrons*, edited by G. T. Rado and H. Suhl (Academic Press Inc., New York, 1963), Vol. I, p. 25.

[4] J. Hubbard, Proc. Roy. Soc. (London) **A276**, 238 (1963).

any reasonably simple approximation in the Bloch representation.

On the other hand, the single-particle Hamiltonian ($H_{\rm sp}$) is best written

$$H_{\rm sp}=\sum_{\rm k}\epsilon_k(n_{\rm k\uparrow}+n_{\rm k\downarrow}), \tag{6}$$

while the Wannier representation

$$H_{\rm sp}=\sum_{\alpha,\beta}V_{\alpha\beta}(c_{\alpha\uparrow}{}^{\dagger}c_{\beta\uparrow}{}^{\dagger}c_{\alpha\downarrow}{}^{\dagger}c_{\beta\downarrow}) \tag{7}$$

obscures the physically important properties of the periodic potential.

The reason for this is, of course, well known. The most important general property of the single-particle Hamiltonian is its periodicity, i.e., its invariance under lattice translations. The Bloch representation is constructed to make full use of this symmetry property.

Quite analogously, the local character of the electron-electron interactions is reflected in the invariance of $H_{\rm int}$ under local spin rotations, e.g., under rotations of the axis of quantization at each site α separately in Eq. (1). This symmetry property of a local-interaction Hamiltonian is quite general and is not restricted to the special nondegenerate case described by $H_{\rm int}$ [Eq. (1)]. In a magnetic state, this implies that the true electron-electron interactions depend only on the magnitude and form of the local spin polarization (in particular, the size of the local moment). They do not depend on the relative orientation of the moments at different sites.[5] The interaction between the relative orientations of the moments is determined by the single-electron Hamiltonian. The purpose of this work was to try to get a better physical understanding as to the way this comes about.

There are, in fact, numerous reasons to believe that complicated nonferromagnetic magnetic states should be important. On the one hand, the extensive work on Overhauser spin-density waves[6] has shown that periodic magnetic deformations of the paramagnetic ground state can be important. Most recently, Penn[7] has shown by explicit numerical calculations on a simple cubic tight-banding model that various complicated magnetic states can have lower energies than the ferromagnetic state.

It can also be shown[8] that the effective magnetic interaction between localized impurity moments can have a very complicated angular dependence.

Our approach in this paper is most closely related to the work of Ref. 7. We discuss the simplest model which can be expected to show the important physical effects, i.e., a nondegenerate band with a localized Coulomb interaction. We therefore assume a Hamiltonian

$$H=H_{\rm sp}+H_{\rm int}, \tag{8}$$

where $H_{\rm sp}$ is given by Eqs. (6) or (7) and $H_{\rm int}$ by Eqs. (1) or (5). In Sec. II the formalism is developed for investigating the ground-state energy of Eq. (8) in a generalized Hartree-Fock (HF) scheme where the magnitude of the local moments is constant but their orientations vary from site to site. We restrict the discussion to ordered states which retain the translational symmetry. In Sec. III the stability of the paramagnetic state is discussed and the importance of the band structure and Fermi-surface geometry are investigated. Our formalism leads to the well-known formulation of this problem discussed, for example, in Refs. 9–13. Some preliminary results of our calculations were discussed in Ref. 4. The results of numerical calculations which illustrate the importance of the various physical effects are also discussed. In Sec. IV the magnetic behavior for finite moments is discussed and results on the stability of the ferromagnetic state are given.

The extension of the present work to degenerate bands will be discussed in a subsequent paper.

II. GREEN'S-FUNCTION FORMALISM

In the following, we restrict our discussion to a nondegenerate band with localized electron-electron interactions at zero temperature. The Hamiltonian is therefore given in the Wannier representation by[4,14]

$$H=\sum_{\alpha,\beta,\sigma}V_{\alpha\beta}c_{\alpha\sigma}{}^{\dagger}c_{\beta\sigma}+U\sum_{\alpha}n_{\alpha\uparrow}n_{\alpha\downarrow}. \tag{9}$$

The direction of spin quantization in Eq. (9) is quite arbitrary, but the Hamiltonian has this form only if one chooses the same direction for all lattice sites α. To describe a state in which the moments at different sites point are in different directions, it is now convenient to transform to a representation in which the spin at each site α is quantized along the direction of the moment at the site. If the original spin operators $c_{\alpha\sigma}$ are quantized along z in a coordinate system x, y, z (common to all sites), and the polar angles in this system of the local direction of quantization z_α at site α are θ_α, ϕ_α, then[8]

$$\begin{aligned}c_{\alpha\uparrow}&=\exp(i\phi_\alpha/2)[\cos\tfrac{1}{2}\theta\, d_{\alpha\uparrow}+\sin\tfrac{1}{2}\theta\, d_{\alpha}],\\ c_{\alpha\downarrow}&=\exp(-i\phi_\alpha/2)[\sin\tfrac{1}{2}\theta\, d_{\alpha\uparrow}-\cos\tfrac{1}{2}\theta\, d_{\alpha\downarrow}].\end{aligned} \tag{10}$$

In Eq. (10), the $d_{\alpha\sigma}$ are annihilation operators of electrons in the Wannier state at $\alpha(w_\alpha)$ and in the spin state σ-quantized along z_α. We now assume an ordered

[5] Note, however, that spin-orbit coupling can reduce the local spin symmetry. This might be important in actual metals but will not be discussed here.

[6] See, e.g., Chap. V of Ref. 2, where this work is reviewed in great detail.

[7] D. R. Penn, Phys. Rev. **142**, 350 (1965).

[8] S. Alexander, Phys. Letters **13**, 6 (1964).

[9] K. Sawada and W. Fukuda, Progr. Theoret. Phys. (Kyoto) **25**, 220 (1961).

[10] N. Fukuda, Phys. Letters **3**, 214 (1963).

[11] F. Iwamoto and K. Sawada, Phys. Rev. **126**, 887 (1962).

[12] M. Tachiki and T. Nagamiya, Phys. Letters **3**, 214 (1963).

[13] P. Lederer and A. Blandin, Phil. Mag. **14**, 363 (1966).

[14] S. Alexander and G. Horwitz, Solid State Commun. **4**, 513 (1966).

state in which all moments lie on a cone and the transverse components form a spiral:

$$\theta_\alpha=\theta, \tag{11}$$

$$\phi_\alpha=\mathbf{q}\cdot\mathbf{R}_\alpha, \tag{12}$$

where $\mathbf{R}_\alpha$ is the radius vector of site α and $\mathbf{q}$ can be any vector[15] in the first Brillouin zone.

This is very general and includes most of the ordered magnetic states with constant moments one could think of. If one wanted to go beyond Bravais lattices, one could extend this by using the irreducible representations of the respective space groups.[11,16]

Substituting Eqs. (11) and (12) in Eq. (10) gives

$$c_\alpha{}^\sigma=(\exp i\tfrac{1}{2}\sigma\mathbf{q}\cdot\mathbf{R}_\alpha)[\hat{\sigma}\cos\tfrac{1}{2}\theta\, d_{\alpha\sigma}+\sin\tfrac{1}{2}\theta\, d_{\alpha-\sigma}], \tag{13}$$

where $-\sigma=\downarrow$ when $\sigma=\uparrow$ and vice versa, and $\hat{\sigma}=+1$ for spin up ($\sigma=\uparrow$) and -1 for spin down ($\sigma=\downarrow$). $H_{\rm int}$ is invariant under local rotations:

$$H_{\rm int}=U\sum_\alpha n_{\alpha\uparrow}n_{\alpha\downarrow}=U\sum_\alpha c_{\alpha\uparrow}{}^\dagger c_{\alpha\uparrow}c_{\alpha\downarrow}{}^\dagger c_{\alpha\downarrow}$$
$$=U\sum_\alpha d_{\alpha\uparrow}{}^\dagger d_{\alpha\uparrow}d_{\alpha\downarrow}{}^\dagger d_{\alpha\downarrow}. \tag{14}$$

For convenience, we will therefore redefine the $n_{\alpha\sigma}$ as the occupation-number operator of the spin state σ along z_α:

$$n_{\alpha\sigma}=d_{\alpha\sigma}{}^\dagger d_{\alpha\sigma}. \tag{15}$$

Substituting (13) in (7) gives for $H_{\rm sp}$

$$H_{\rm sp}=\sum_{\alpha,\beta}V_{\alpha\beta}c_{\alpha\sigma}{}^\dagger c_{\beta\sigma}$$
$$=\sum_{\alpha,\beta,\sigma}V_{\alpha\beta}\{\exp[-i\tfrac{1}{2}\hat{\sigma}\mathbf{q}\cdot(\mathbf{R}_\alpha-\mathbf{R}_\beta)]\}$$
$$\times[\cos^2(\tfrac{1}{2}\theta)\, d_{\alpha\sigma}{}^\dagger d_{\beta\sigma}+\sin^2(\tfrac{1}{2}\theta)d_{\alpha-\sigma}{}^\dagger d_{\beta-\sigma}$$
$$+\tfrac{1}{2}\hat{\sigma}\sin\theta\,(d_{\alpha\sigma}{}^\dagger d_{\beta-\sigma}+d_{\alpha-\sigma}{}^\dagger d_{\beta\sigma})]. \tag{16}$$

We now want to investigate the properties of the Hamiltonian (8) in a generalized HF scheme, assuming a constant magnitude for the local moments, i.e.,

$$\langle n_{\alpha\sigma}\rangle=n_\sigma, \tag{17}$$

where $\langle n_{\alpha\sigma}\rangle$ is the expectation value of the operator $n_{\alpha\sigma}$ for given $\mathbf{q}$ and θ. It is easiest to do this using the two-time single-particle retarded Green's function[17] (Im$\epsilon>0$):

$$G_{\alpha\beta}{}^{\sigma,\sigma'}(\epsilon)=\langle\langle d_\alpha;\, d_\beta{}^\dagger\rangle\rangle_\epsilon, \tag{18}$$

which obey the equations of motion

$$\epsilon\langle\langle d_{\alpha\sigma};\, d_{\beta\sigma'}{}^\dagger\rangle\rangle_\epsilon=\langle(d_{\alpha\sigma}d_{\beta\sigma'}{}^\dagger)_+\rangle/2\pi+\langle\langle(d_{\alpha\sigma'}H);\, d_{\beta\sigma'}{}^\dagger\rangle\rangle_\epsilon \tag{19}$$

with Hartree-Fock decoupling of the two-particle Green's functions which appear on the right side. For this we need the commutation

$$(d_{\alpha\sigma},\, H)=Un_{\alpha-\sigma}d_{\alpha\sigma}{}^\dagger$$
$$+\sum_\beta[V_{\alpha\beta}\mid\exp[-i\hat{\sigma}\mathbf{q}\cdot(\mathbf{R}_\alpha-\mathbf{R}_\beta)/2]\cos^2\tfrac{1}{2}\theta$$
$$+\exp[+i\hat{\sigma}\mathbf{q}\cdot(\mathbf{R}_\alpha-\mathbf{R}_\beta)]\sin^2\tfrac{1}{2}\theta\mid d_{\beta\sigma}$$
$$+\tfrac{1}{2}V_{\alpha\beta}\sin\theta\{\exp[-i\mathbf{q}\cdot(\mathbf{R}_\alpha-\mathbf{R}_\beta)\tfrac{1}{2}]$$
$$-\exp[i\mathbf{q}\cdot(\mathbf{R}_\alpha-\mathbf{R}_\beta)\tfrac{1}{2}]\}d_{\beta-\sigma}]. \tag{20}$$

Now the Hartree-Fock approximation means that we decouple the first term on the right side,

$$n_{\alpha-\sigma}d_{\alpha\sigma}=d_{\alpha\sigma}\langle n_{\alpha-\sigma}\rangle. \tag{21}$$

Equation (21) is the complete HF decoupling

$$[\langle d_{\alpha\sigma}{}^\dagger d_{\alpha-\sigma}\rangle=0],$$

because we have assumed that we have chosen the axis of quantization along the direction of the local moment.[18]

Now we make a Bloch transformation:

$$d_{\mathbf{k}\sigma}=(1/\sqrt{N})\sum_\alpha\exp(-i\mathbf{k}\cdot\mathbf{R}_\alpha)d_{\alpha\sigma}, \tag{22}$$

where $d_{\mathbf{k}\sigma}$ is an annihilation operator for an electron of momentum $\mathbf{k}$ with spin on the cone.[19] Using (17) in (21) and substituting in (20), leads to

$$(d_{\mathbf{k}\sigma},\, H)=(Un_{-\sigma}+A_{\mathbf{k},\mathbf{q}}+\hat{\sigma}D_{\mathbf{k},\mathbf{q}}\cos\theta)d_{\mathbf{k}\sigma}$$
$$+\sin\theta D_{\mathbf{k},\mathbf{q}}d_{\mathbf{k}-\sigma}, \tag{23}$$

where

$$A_{\mathbf{k},\mathbf{q}}=\tfrac{1}{2}(\epsilon_{\mathbf{k}+\mathbf{q}/2}+\epsilon_{\mathbf{k}-\mathbf{q}/2}),$$
$$D_{\mathbf{k},\mathbf{q}}=\tfrac{1}{2}(\epsilon_{\mathbf{k}+\mathbf{q}/2}-\epsilon_{\mathbf{k}-\mathbf{q}/2}). \tag{24}$$

Finally one gets for

$$G_{\mathbf{k}\mathbf{k}'}{}^{\sigma\sigma'}=\langle\langle d_{\mathbf{k}\sigma},\, d_{\mathbf{k}'\sigma'}{}^\dagger\rangle\rangle_\epsilon \tag{25}$$

the result

$$(g_{\mathbf{k}}{}^\sigma)^{-1}G_{\mathbf{k}\mathbf{k}'}{}^{\sigma\sigma'}=\delta(\mathbf{k}\mathbf{k}')\delta(\sigma\sigma')/2\pi+\sin\theta\, D_{\mathbf{k}\mathbf{q}}G_{\mathbf{k}\mathbf{k}'}{}^{-\sigma\sigma'}, \tag{26}$$

where

$$g_{\mathbf{k}}{}^\sigma=(\epsilon+is-Un_{-\sigma}-A_{kq}-\hat{\sigma}D_{kq}\cos\theta)^{-1}. \tag{27}$$

In practice, we are only interested in the diagonal elements of G. Solving (26) for these gives

$$G_{\mathbf{k}\mathbf{k}}{}^{\sigma\sigma}=(1/2\pi)[(g_{\mathbf{k}}{}^\sigma)^{-1}-D_{\mathbf{k}\mathbf{q}}{}^2\sin^2\theta\, g_{\mathbf{k}}{}^{-\sigma}]^{-1}. \tag{28}$$

Now the Hartree-Fock internal energy per electron is given by

$$E=N^{-1}\int^\mu\epsilon d\epsilon\ 2\ \mathrm{Im}\sum_{\mathbf{k}}\sum_\sigma(G_{\mathbf{k}\mathbf{k}}{}^{\sigma\sigma})+Ud^2, \tag{29}$$

[15] In general, $\mathbf{q}$ is not parallel to z.

[16] S. Alexander, Phys. Rev. **127,** 420 (1962).

[17] O. N. Zubarev, Usp. Fiz. Nauk **71,** (1960) [English transl.: Soviet Phys.—Usp. **3,** 320 (1960)].

[18] See Appendix A for a proof that there is such a direction for any magnetic state. For a nonmagnetic state, results are rotational invariant and do not depend on quantization direction.

[19] In fact,

$$dx_\sigma=\hat{\sigma}\cos\tfrac{1}{2}\theta\, C_{\mathbf{k}+\hat{\sigma}\mathbf{p}/2}+\sin\tfrac{1}{2}\theta\, C_{\mathbf{k}-\hat{\sigma}\mathbf{p}/2},$$

which follows from the connection between linear and cone-spin quantization (see, e.g., Ref. 2).

where the Fermi level μ is determined by

$$n=(2N)^{-1}\int^{\mu} d\epsilon\, 2\ \mathrm{Im}\sum_{\mathbf{k}}\sum_{\sigma}(G_{\mathbf{kk}}{}^{\sigma\sigma}). \quad (30)$$

We have introduced in (29) and (30) the notation

$$n=\tfrac{1}{2}(n_{\uparrow}+n_{\downarrow}),$$
$$d=\tfrac{1}{2}(n_{\uparrow}-n_{\downarrow}). \quad (31)$$

With this notation

$$U\langle n_{\uparrow}\rangle\langle n_{\downarrow}\rangle=U(n^2-d^2), \quad (32)$$

and we have omitted the irrelevant constant $-Un^2$ on the right side of (29).

In addition to (29) and (30), self-consistency clearly requires that

$$d=(2N)^{-1}\int^{\mu} d\epsilon\, 2\ \mathrm{Im}\sum_{\sigma}\sum_{\mathbf{k}}(G_{\mathbf{kk}}{}^{\sigma\sigma}{}_{\sigma}). \quad (33)$$

The $G_{\mathbf{kk}}{}^{\sigma\sigma}(\epsilon)$ [Eq. (26)] depend explicitly on the d, $\mathbf{q}$, and θ as parameters. As a result, (29) defines the energy as a function of these arguments. The self-consistency requirement (33) is, in fact, identical with the requirement that the energy should be extremal with respect to d.

It should be stressed that our discussion is limited to zero temperature. One could add the proper Fermi functions in the integrals to obtain the internal energy from (29), n, and d [Eqs. (30), (33)] at finite temperatures. To investigate the behavior of the system at finite temperatures, one would, however, have to replace the internal energy (29) by an expression for the free energy. This becomes considerably more complicated and will not be attempted here.[20]

The physical states described by different values of the arguments $\mathbf{q}$ and θ are not necessarily distinct. The resulting properties of $E(d, \theta, \mathbf{q})$ as a function of its arguments are discussed in Appendix B.

We now want to study the behavior of the HF energy in some more detail. It is then convenient to rewrite the integrals (29) and (30). Now

$$\sum_{\sigma} G_{\mathbf{kk}}{}^{\sigma\sigma}=G_{\mathbf{k}}{}^{+}+G_{\mathbf{k}}{}^{-}, \quad (34)$$

where

$$G_{\mathbf{k}}{}^{\pm}=(1/2\pi)(\epsilon-is-Un-A_{\mathbf{kq}}\mp L_{\mathbf{kq}})^{-1}, \quad (35)$$

and

$$L_{\mathbf{kq}}=[(Ud-D_{\mathbf{kq}}\cos\theta)^2+D_{\mathbf{kq}}{}^2\sin^2\theta]^{1/2}. \quad (36)$$

Substituting (34) in (29) gives

$$E(d, \mathbf{q}, \theta)=\int^{\mu}\epsilon\, 2\ \mathrm{Im}(G^{+}+G^{-})\,d\epsilon+Ud^2, \quad (37)$$

which should be minimized with the subsidiary condition that

$$n=\int^{\mu}\mathrm{Im}(G^{+}+G^{-})\,d\epsilon. \quad (38)$$

In (37) and (38) the omission of the subscript $\mathbf{k}$ implies summation over $\mathbf{k}$. We will use this notation throughout this paper.

The separation (34) demonstrates that, in a sense, one can always describe the HF ground state for arbitrary $\mathbf{q}$ and θ in terms of a splitting into an "upper" band described by the G^{+} and a lower band described by the G^{-}. It is, however, important to remember that the "band splitting" for given $\mathbf{q}$ and θ depends explicitly on $\mathbf{k}$ and has a complicated Ud dependence. G^{+} and G^{-} describe the true HF poles of the single-electron states in a *partially* polarized state and not the spin-up and -down states.

Notice the nonvanishing of the $G_{\mathbf{kk}'}{}^{\sigma-\sigma}$ is what produces the partial polarization of the bands. On the other hand,

$$(1/N)\sum_{\mathbf{kk}'}\mathrm{Im}G_{\mathbf{kk}'}{}^{\sigma-\sigma}=\langle c_{\alpha\sigma}{}^{\dagger}c_{\alpha-\sigma}\rangle$$

can be shown to vanish, as is necessary for consistency.

Equations (37) and (38) define the HF energy as a function of the free parameters d, $\mathbf{q}$, and θ. For given band structure $\epsilon_{\mathbf{k}}$, electron number $2n$, and U, we want the extrema of this function. The calculation of the extremum conditions from (37) and (38) is quite straightforward. The results are, however, rather cumbersome and are given in Appendix C.

In principle, it would, of course, be possible to use Eqs. (37) and (38) and the results derived in Appendix C to find the actual extrema of the HF energy. We will not attempt such a survey and shall restrict our discussion to certain limiting cases.

In Sec. III we discuss the stability of the paramagnetic state ($d=0$) and its relationship to the band structure. In Sec. IV we investigate the stability of the ferromagnetic state ($d\neq 0$, $\theta=0$) as compared to conical spirals.

III. STABILITY OF THE PARAMAGNETIC STATES

The paramagnetic state $d=0$ is always an extremum of the energy, i.e.,

$$(\partial E/\partial d)_{d=0}=0. \quad (39)$$

In fact, the physical state is independent of $\mathbf{q}$ and θ, and these parameters only serve to relabel the $G_{k}{}^{\pm}(\epsilon)$. As pointed out in Appendix B, the energy of this state is independent of $\mathbf{q}$ and θ, so that the stability of the paramagnetic state is completely determined by $(\partial^2 E/\partial d^2)\,|_{\mathbf{q},\theta;d=0}$.

For $d=0$, Eq. (C3) becomes

$$(\partial^2 E/\partial d^2)_{d=0}=2U^2[1/U-\sin^2\theta A_0(\mathbf{q})-\cos^2\theta\rho_0(\mu)], \quad (40)$$

[20] It can be shown quite generally that the finite-temperature expression resulting from Eq. (33) is equivalent to the condition that the Hartree-Fock free energy be extremal with respect to d. We do not know of any analogous results for the extremum conditions of the free energy with respect to q and θ.

where $A_0(q)$ is the well-known integral

$$A_0(\mathbf{q}) = -\int^{\epsilon_k<\mu} d\mathbf{k}(\epsilon_{\mathbf{k}}-\epsilon_{\mathbf{k}+\mathbf{q}})^{-1}, \tag{41}$$

and

$$\rho_0(\mu) = \tfrac{1}{2}\times 2\ \mathrm{Im}[G^+(\mu)+G^-(\mu)] \tag{42}$$

is the density of states at the Fermi surface μ for one spin direction in the paramagnetic state. The derivation of (40) from (C3) is quite straightforward when one remembers that

$$\epsilon_{\mathbf{k}} = \epsilon_{-\mathbf{k}}. \tag{43}$$

The result is identical with that of Refs. 9–13.

The investigation of the stability of the paramagnetic state is obviously interesting only in situations where the final polarization d is reasonably small, that is, for small U. It is therefore simplest to consider U as a parameter and look for the maximum of the right side of (40) as a function of $\mathbf{q}$ and θ. Because

$$A_0(0) = \rho(\mu), \tag{44}$$

it is sufficient to consider the case of $\theta = \frac{1}{2}\pi$ and look for the maximum of $A_0(\mathbf{q})$ [Eq. (41)].[21]

The paramagnetic state becomes unstable with respect to a spiral of wave vector $\mathbf{q}$ when

$$UA_0(\mathbf{q}) \geq 1$$

[(see Eq. 40)]. At the maximum of $A_0(\mathbf{q})$, this will occur for the smallest U. For continuity reasons, one therefore expects the small-moment (small U) magnetic states to be those for which $A_0(\mathbf{q})$ is large. When the magnetization is large, this is of course no longer a valid argument. It is shown in Sec. IV that the large-moment behavior is radically different from that described by $A_0(\mathbf{q})$. In this section we restrict ourselves to a discussion of $A_0(\mathbf{q})$ and the resulting small-moment behavior.

The integral $A_0(\mathbf{q})$ describes the wave-vector-dependent static susceptibility of the electron gas and it also appears in other problems concerning magnetism in metals. In particular, the conduction electron polarization by (nuclear or electronic) local moments and the resulting effective coupling between such moments is determined by the same expression.

Even though this integral has been discussed by numerous authors (e.g., in Ref. 12) it seems that the importance of specific band-structure effects has not been considered sufficiently. Recently, the authors have discussed the extreme importance of umklapp processes and saddle points.[14] It is nevertheless of interest to discuss the properties of this quantity which dominates the magnetic properties of the paramagnetic state in more detail.

[21] If the maximum is ferromagnetic it is independent of θ. Any nonferromagnetic maximum must come from $q\neq 0$ and hence for an $A_0(q)>A_0(0)=\rho(\mu)$. This is maximized by $\theta=\frac{1}{2}\pi$.

A. Free-Electron Behavior

For free electrons,

$$\epsilon_k = k^2. \tag{45}$$

It is possible to evaluate $A_0(\mathbf{q})$ explicitly;

$$A_0^{\mathrm{free}}(\mathbf{q}) = \frac{-\pi}{q}\left[(k_F^2-\tfrac{1}{4}q^2)\ln\left|\frac{k_F-\frac{1}{2}q}{k_F+\frac{1}{2}q}\right| - qk_F\right], \tag{46}$$

which only depends on the magnitude $q=|\mathbf{q}|$. This is a smooth monotonic decreasing function of q with a maximum at $\mathbf{q}=0$.

Within our model, this means that the ferromagnetic state is favored for free electrons (45) at least for small magnetization.

For our purposes it is important to stress that $A_0(q)$ in (46) varies relatively slowly for $q<2k_F$ and has a logarithmically divergent (negative) derivative for $q=2k_F$. As a result, $A_0(q)$ is large and fairly constant below $2k_F$ and very small for q appreciably larger. Thus, $A_0(0)/A_0(2k_F)=2$.

Physically, this reflects the fact that spiral wave packets of wave vectors $q<2k_F$ can be formed from states in the vicinity of the Fermi surface.[22] This is not possible for larger q. The free electron $A_0^{\mathrm{free}}(q)$ becomes small for large q because the denominators in the integrand in (41) become large. The energy $\epsilon_{\mathbf{k}+\mathbf{q}}$ is a monotonic increasing function of $|\mathbf{k}+\mathbf{q})$ and therefore becomes large for large $\mathbf{q}$.

B. Umklapp Processes

For Bloch electrons in a crystal, this is no longer true because the energies $\epsilon_{\mathbf{k}}$ are periodic functions of $\mathbf{k}$. Whenever $\mathbf{k}+\mathbf{q}$ falls outside the Brillouin zone, the energy $\epsilon_{\mathbf{k}+\mathbf{q}}$ is replaced by the (in general) smaller energy $\epsilon_{\mathbf{k}+\mathbf{q}-\mathbf{K}}$ where $\mathbf{K}$ is a reciprocal lattice vector. As a result, $A_0(q)$ is increased for large q.

From the qualitative features of (46), one would expect this effect to become important only for $q<2k_F$ for which $A_0^{\mathrm{free}}(q)$ is already appreciable. As $\mathbf{q}$ in a crystal is (in this context) necessarily inside the zone ($\mathbf{q}\leq\frac{1}{2}\mathbf{K}$), this implies that umklapp processes should become important only for

$$k_F \geq \tfrac{1}{4}\mathbf{K}, \tag{47}$$

where $\mathbf{K}$ is a suitable reciprocal lattice vector.

This is very nicely illustrated by the following simple model. We assume free-electron dispersion relations for the energy (45) and replace the crystalline potential by umklapp processes at a simple cubic zone boundary.[23] For simplicity, we moreover restrict ourselves to wave vectors $\mathbf{q}$ along the principal tetragonal axis of the cube.[24] It is then possible to calculate $A_0(q)$ analytically for $k_F\leq\frac{1}{2}K$.

[22] See Ref. 19.

[23] A very similar model was discussed by Tachiki and Nagamiya in Ref. 12, who used more complicated zone boundaries.

[24] This is purely a matter of mathematical convenience and does not imply that these are actually the most favorable directions.

One has

$$A_0(q)=A_0^{\text{free}}(q), \qquad |\mathbf{q}|\leq|\tfrac{1}{2}K-\mathbf{k}_F|, \quad (48a)$$

$$A_0(q)=F(q)+F(K-q), \qquad |\mathbf{q}|\geq|\tfrac{1}{2}K-\mathbf{k}_F|, \quad (48b)$$

where

$$F(x)=(\pi/x)[(k_F^2-x^2/4)\ \ln|\,(k_F-\tfrac{1}{2}x)/(\tfrac{1}{2}K-\tfrac{1}{2}x)\,| -\tfrac{1}{2}k_F(k_F+x)+\tfrac{1}{2}(\tfrac{1}{2}K-x)(\tfrac{1}{2}K-2x)]. \quad (49)$$

Some typical curves of $A_0(q)$ for different values of k_F/K are given in Fig. 1. It can be seen that for small values of k_F/K one gets essentially the free-electron behavior A_0^{free}. For $k_F/K>\frac{1}{4}$, a second maximum appears at the zone boundary $q=\frac{1}{2}K$.

It is clear from (49) that $F(x)$ has a logarithmically infinite negative derivative (PIS) for $x=2k_F$. In fact, all derivatives of $F(x)$ diverge at this point. Thus $F(q)$ has an infinite negative slope for $q=2k_F$ similar to that of $A_0^{\text{free}}(q)$, and $F(K-q)$ has an infinite positive slope when

$$|\mathbf{K}-\mathbf{q}|=2k_F. \quad (50)$$

Physically, we are only interested in q within the zone, i.e., $q<\frac{1}{2}K$. There is, therefore, only one point of infinite slope in $A_0(q)$ [Eqs. (48)]. When

$$k_F\leq\tfrac{1}{6}K \quad (51)$$

this point is in the free-electron region (48a). For

$$\tfrac{1}{6}K<k_F<\tfrac{1}{4}K \quad (52)$$

there is still a point of infinite negative slope (negative PIS) due to $F(q)$ in (48b). However, for

$$k_F>\tfrac{1}{4}K \quad (53)$$

one only gets the point of infinite positive slope (positive PIS) due to $F(K-q)$, so that $A_0(q)$ is bound to have a maximum for

$$q>K-2k_F. \quad (54)$$

On the other hand, $A_0(q)$ in (48b) necessarily has an extremum on the zone boundary where

$$q=K-q=\tfrac{1}{2}K, \quad (55)$$

and this is usually the only possible position of the maximum we have described.[25]

It is of interest to note that the transition from the monotonic regime ($k_F<\frac{1}{4}K$) to that with an antiferromagnetic maximum is somewhat peculiar. All odd derivatives of $A_0(q)$ given by (48b) vanish on the boundary because of (55). However, for $k_F=\frac{1}{4}K$ the even derivatives diverge there so that the minimum disappears as a very-narrow "well." The maximum also appears as a narrow step near $q=\frac{1}{2}K$. This can be seen, for example, in the curves $k_F/K=0.24625$ and 0.26125 in Fig. 1.

[25] See, however, the subsequent discussion.

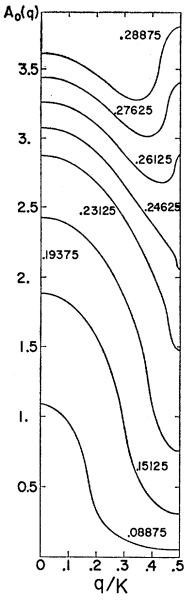

FIG. 1. Computed curves of $A_0(\mathbf{q})$ for free electrons with umklapp processes at a cubic zone boundary and $\mathbf{q}$ perpendicular to the boundary. The curves are plots of Eq. (48). The numerial labels on each curve indicate the value of k_f/K. Note in particular the change from a negative infinite slope at $q=2k_f$ for the curve with $k_f/K=0.24625$ to a positive infinite slope at $(K-q)=2\mathbf{k}_f$ for $k_f/K=0.26125$.

Another intriguing feature of this model is that when

$$k_F=\tfrac{1}{2}K, \quad (56)$$

so that the Fermi surface touches the zone boundary, one finds

$$A_0(q)=\pi K \quad (57)$$

independent of q. In a way, this is a fortuitous feature of the model which is certainly very artificial when $k_F\sim\frac{1}{2}K$. It does, however, reflect a real effect. As the Fermi surface approaches the zone boundary, the point of infinite positive slope ($q=K-2k_F$) approaches $q=0$, and it disappears altogether when the surface touches the boundary. As a result, $A_0(q)$ becomes very flat and moreover the maximum at the boundary disappears.

In the region we are actually interested in, i.e., near $k_F/K=0.25$, one really expects this sort of free-electron model to be quite meaningful because the Fermi surface is still very far from the zone boundaries. It seems clear from the physics of this sort of problem that the only really significant feature is the effect of umklapp processes on the mixing of states near the Fermi surface. The detailed structure in relatively high-energy states near the zone boundary can not possibly have a large effect. It will be shown later (Sec. III D) that numerical calculations with quite different band structures give exactly the same results.

A much more serious limitation is, certainly, the fact that we have limited ourselves to $\mathbf{q}$ perpendicular to the zone boundary so that the effect of tangential components of $\mathbf{q}$ is not considered at all.

C. Saddle Points

It is well known that the existence of saddle points in the energy has important effects on the properties

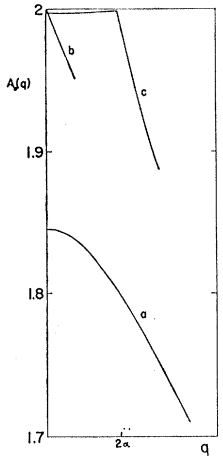

FIG. 2. Computed curves of the transverse contribution of a saddle point to $A_0(q)$. Details are given in Appendix D. In curve a the Fermi level is below the sp, curve b is computed for $\mu=\epsilon_{sp}$, and curve c when there is a neck ($\mu>\epsilon_{sp}$). Note the discontinuity of the derivative of $A_0(q)$ when q is equal to the diameter of the neck. All curves are computed with q perpendicular to the axis of the sp.

of band electrons. For our purposes, the most important feature is the appearance of "necks" in the Fermi surface when the Fermi energy is above the sp.

For simplicity, we assume that the expansion of the energies ϵ_k around the saddle point has the form[26]

$$\epsilon=\epsilon_k-\epsilon_{sp}=x^2-y^2+z^2, \tag{58}$$

where x, y, and z are the components of

$$\mathbf{k}-\mathbf{k}_{sp} \tag{59}$$

along suitable directions in $\mathbf{k}$ space, and ϵ_{sp} and $\mathbf{k}_{sp}$ are the energy and crystal momentum of the sp, respectively.

In the vicinity of the sp the constant-energy surfaces are thus hyperboloids with the axis y. When

$$\epsilon<0,$$

these are two-sheeted hyperboloids, while for

$$\epsilon\geq 0,$$

a neck is formed around the sp and the surfaces are single-sheeted hyperboloids.

We want the contribution to $A_0(q)$ from the vicinity of the saddle point, i.e.,

$$A_0^{sp}(\mathbf{q})=-\int'^{k\epsilon R}\frac{\theta(\epsilon_k-\mu)}{\epsilon_k-\epsilon_{k+q}}d\mathbf{k}, \quad \theta(\epsilon_k-\mu)=1, \quad \epsilon_k<\mu$$
$$=0, \quad \epsilon_k>\mu \tag{60}$$

where the region R is sufficiently small so that (58) is valid for all ϵ_k and ϵ_{k+q} in (60). This also implies that $\mathbf{q}$ has to be small. Obviously, $A_0^{sp}(\mathbf{q})$ has no meaning for large $\mathbf{q}$.

There are two distinct cases of interest, namely, the axial case

$$q=q_y \tag{61}$$

[26] The extension to the general case is quite straightforward but would complicate the mathematical argument.

and the case of $\mathbf{q}$ in the x-z plane, e.g.,

$$q=q_z. \tag{62}$$

The axial case is very similar to the situation we considered in Sec. III B. The Fermi surface has two opposing convex parts, and we are interested in the effect of mixing electronic states in the two opposing parts. It is convenient to choose a cylindrical region R such that

$$-a\leq q_a\leq a,$$
$$q_x^2+q_z^2<r^2, \tag{63}$$

where r is large enough so that

$$\mu+a^2<r^2. \tag{64}$$

Then for

$$\mu-\epsilon_{sp}=-\alpha^2\leq 0, \tag{65}$$

$$A_0^{sp}(q)=(1/2q)\left[(\alpha^2-(q/2)^2)\ln\left|\frac{a-\frac{1}{2}q}{a+\frac{1}{2}q}\right|\right.$$
$$\left.-\ln\left|\frac{\alpha-\frac{1}{2}q}{\alpha+\frac{1}{2}q}\right|-(a-\alpha)q\right]; \quad q=q_y \tag{66}$$

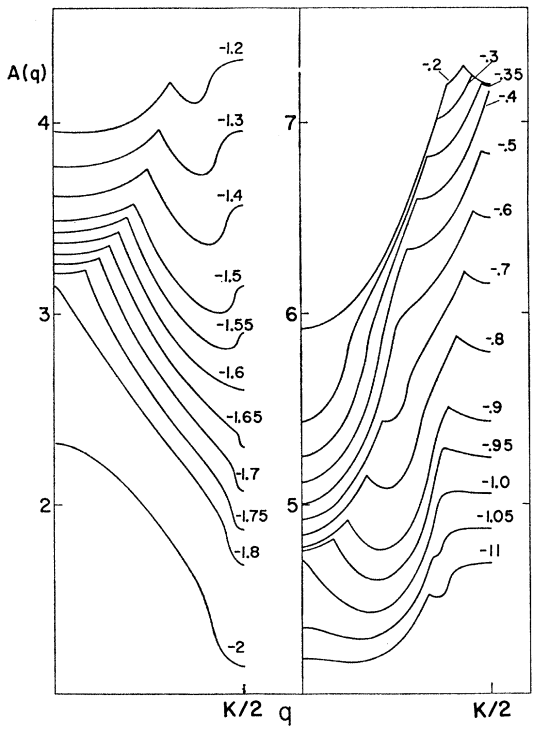

FIG. 3. Curves of $A(q)$ for the orthorhombic band structure of Table I and $q=q_z$. The vertical scale is abritrary but is the same for all curves given. The numerical labels on the curves indicate the position of the Fermi level in the band for which each curve was computed. Note the appearance of discontinuities in the slope due to the saddle points at $\mu=-1.8$ [100] and $\mu=-1$ [010]. A PIS appears above $\mu=-1.6$ due to umklapp processes. Note also the effect of the relative positions of the two SPD's and of the divergence of the slope.

and for

$$\mu-\epsilon_{sp}=\alpha^2\geq 0, \tag{67}$$

$$A_0^{sp}(q)=(1/2q)\left[(\alpha^2+(q/2)^2)\ln\left|\frac{a+\frac{1}{2}q}{a-\frac{1}{2}q}\right|-aq\right], \tag{68}$$

where

$$q=q_y.$$

Equation (66) is very similar to Eqs. (48) and displays an infinite positive derivative when

$$\alpha=\tfrac{1}{2}q,$$

which we discussed in Sec. III B. The present calculation is clearly meaningful only for $q/a\ll 1$, so that the large q behavior is not included.

As a is an arbitrary constant, the result above the saddle point (68) is not very meaningful. It shows, however, that there is no point of infinite slope in $A_0(q)$ along the axis of the sp in this region. As a result, the antiferromagnetic maximum on the zone boundary disappears above the saddle point. This is indeed shown in all numerical calculations (see Sec. III D).

The case of a transverse q [Eq. (62)] is much more interesting. As pointed out in Ref. 14, one expects an important effect above the sp when q is equal to the diameter of the neck. Unfortunately, the mathematics is somewhat involved; it is discussed in Appendix D. It is shown there that the region near the saddle point causes a discontinuous negative change in in the derivative $dA_0(q)/dq$ when q is equal to the diameter of the neck.

In Fig. 2 we show the results of a numerical evaluation of $A_0^{sp}(q)$ for a cubic region near the saddle point.

Curve a is for $\mu<\epsilon_{sp}$. A_0^{sp} is a monotonic decreasing function of q with a maximum at $q=0$. Curve b is calculated for $\mu=\epsilon_{sp}$, and curve c for

$$\mu=\alpha^2>\epsilon_{sp}. \tag{69}$$

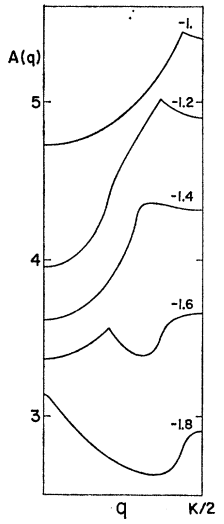

FIG. 4. Same as Fig. 3 except that $q=q_y$. Vertical $A(q)$ scale is the same in both figures.

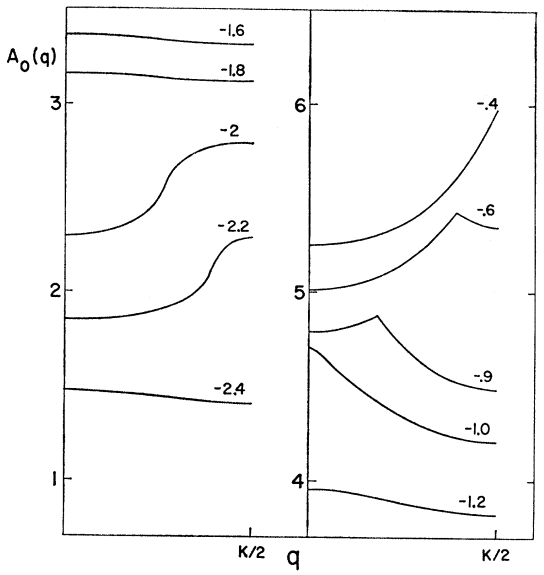

FIG. 5. Same as Figs. 3 and 4 for $q=q_x$. Note the extreme flatness of the curves at -2.4, -1.8, and -1.6 when there are no logarithmic singularities in the derivative and no transverse saddle points.

It can be seen that A_0^{sp} is a slowly increasing function for

$$q<2\alpha, \tag{70}$$

and that it decreases rapidly above 2α. As shown in Appendix D, there is a discontinuity in the derivative at $q=2\alpha$ when q is equal to the diameter of the neck. The general nature of the discontinuity is similar to that found in the density of states near a saddle point except for the fact that the derivatives of $A_0^{sp}(q)$ are finite on both sides of the discontinuity. It should also be noted that for $\alpha=0$, $A_0^{sp}(q)$ seems to approach $q=0$ with a finite slope [Fig. 2(b)]. In Figs. 3–5 we show the computed curves of $A_0(q)$ for an orthorhombic tight-binding band structure. It can be seen that the behavior near saddle points is very similar to that of Fig. 2.

D. Calculations with Model Band Structures

To illustrate the above arguments and get a better feeling for the behavior of the wave-vector-dependent susceptibility, we have calculated $A_0(q)$ for a number of simple tight-binding band structures. The structures considered were all of the types[27]

$$\epsilon_k=-A\cos k_x-B\cos k_y-C\cos k_z. \tag{71}$$

They therefore refer to simple-cubic crystal structures when

$$A=B=C, \tag{72}$$

to a simple-tetragonal structure when

$$A=B\neq C, \tag{73}$$

[27] Note that k_x, k_y, and k_z are here taken as dimensionless quantities defined in terms of the respective reciprocal lattice vectors.

TABLE I. Values of A, B, and C in the tight-binding structures $\epsilon_k = -A\cos k_x - \cos k_y - C\cos k_z$ used in numerical calculations and positions of electron saddle points. Energy units are $\frac{1}{6}$ of band width.

Type	A	B	C	Saddle points 100	010	001
Cubic	1	1	1	−1.0	−1.0	−1.0
Tetragonal I	0.8	0.8	1.4	−1.4	−1.4	−0.2
Tetragonal II	1.2	1.2	0.6	−0.6	−0.6	−1.8
Orthorhombic	0.6	1.0	1.4	−1.8	−1.0	−0.2

and to a simple-orthorhombic structure when

$$A \neq B \neq C. \tag{74}$$

The values of A, B, and C actually used are given in Table I.

Because of the symmetry of $A_0(q)$ [Eq. (41)] between electrons and holes, and because for these band structures

$$\epsilon_{k_x,k_y,k_z} = -\epsilon_{\pi-k_x,\pi-k_y,\pi-k_z}, \tag{75}$$

it is sufficient to consider only the lower half of the band.

We have calculated $A_0(\mathbf{q})$ for a $\mathbf{q}$ along the principal axis of the structure, i.e., of the type

$$(0,\ 0,\ q),\quad (0,\ q,\ 0),\quad (q,\ 0,\ 0). \tag{76}$$

These directions were chosen because of mathematical convenience and because they display the effects of umklapp processes and saddle points most clearly. A much more detailed sampling of the Brillouin zone would, of course, be required if one wanted to find the true maximum of $A_0(q)$ in the zone. It should, however, be stressed that our calculation is sufficient to determine if the homogeneous ferromagnetic susceptibility $[A_0(0)]$ is a maximum. In all cases where $A_0(q)$ has larger values for some $q \neq 0$, it follows that the initial magnetic instability does not occur at $q=0$. In such cases, Overhauser spin-density waves of finite q or antiferromagnetic spin-density waves on the zone boundary are the dominant magnetic instabilities of the electron gas.

In Figs. 6–9, we have plotted the values of q for which $A_0(q)$ is largest as a function of the position of the Fermi level in the bands for all four band structures given in Table I and along the distinct directions of the type (76). In cases where $A_0(q)$ has more than one local maximum or locally largest value, the lower values are indicated by dashed curves. On all curves the shaded areas indicate regions where

$$A_0(q) < A_0(0),$$

and the white areas regions where

$$A_0(q) > A_0(0).$$

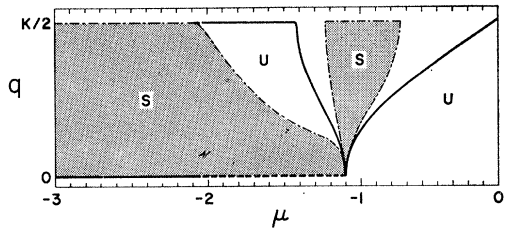

FIG. 6. Positions of maxima of $A_0(q)$ and regions for which $A_0(q) > A_0(0)$ as a function of the position of the paramagnetic Fermi level μ in a simple-cubic tight-binding band for q along [100]. Solid curves indicate the q for which $A_0(q)$ is largest for a given μ. When there are additional local maxima, these are indicated by dashed curves. The shaded areas S are regions for which $A_0(q) < A_0(0)$ and the white areas U regions where $A_0(q) > A_0(0)$ always for the same μ. Only the lower half of the band is shown. The upper half is completely symmetrical. Note the cusp at the saddle point ($\mu = -1$) where the longitudinal PIS disappears and the SPD due to trasverse neck appears.

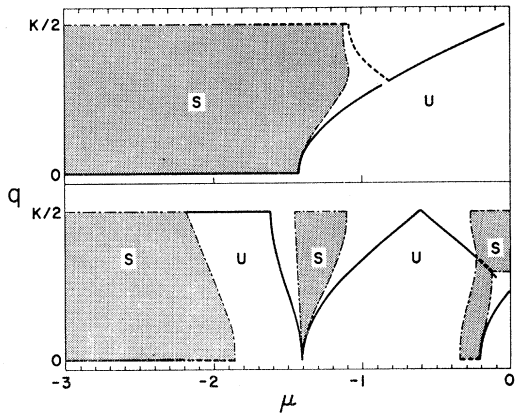

FIG. 7. Same as Fig. 6 for the tetragonal case I (Table I). The upper drawing is for q along the tetragonal axis [001] and shows umklapp PIS above $\mu = -1.6$ and the effect of the degenerate saddle point at -1.4. The lower drawing is for q along [100] and shows umklapp above -2.2 and the two saddle points at -1.4 and -0.2.

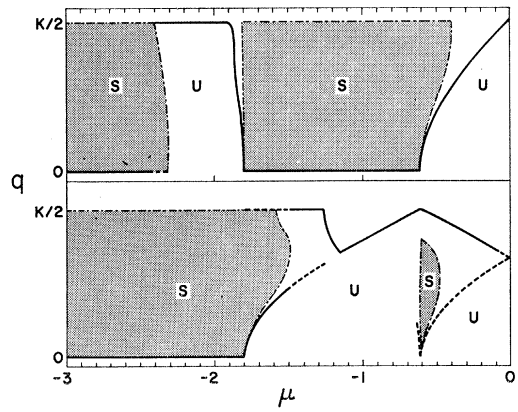

FIG. 8. Same as Fig. 7 for tetragonal structure II. Note the disappearance of the z-axis umklapp processes at the z saddle point ($\mu = -1.8$) in the upper curve.

As discussed in Secs. III B and III C above, the behavior of $A_0(q)$ is dominated by the points of infinite slope (PIS) due to free-electron and umklapp processes, and by the necks around saddle points.

Thus for q along the x direction, there will be a point of infinite negative slope (NPIS) at

$$q=2k_f{}^x=2\cos^{-1}[(-\mu-B-C)/A] \tag{77}$$

when

$$k_f{}^x<\tfrac{1}{2}\pi, \tag{78}$$

and therefore

$$d<-B-C. \tag{78'}$$

Above this, there is a point of positive infinite slope (PPIS) for

$$A-B-C\geq\mu>-B-C \tag{79}$$

at

$$q=2\pi-2k_f{}^x. \tag{80}$$

Above the saddle point at

$$\mu=A-B-C, \tag{81}$$

the Fermi surface touches the zone boundary in the x direction at $(\pi, 0, 0)$, and there is no point of infinite slope in this direction.

We also have to consider the effect of saddle points along y and z. These appear at [28]

$$(0, \pi, 0);\quad \epsilon_{\rm sp}{}^y=-A+B-C, \tag{82a}$$

and at

$$(0, 0, \pi);\quad \epsilon_{\rm sp}{}^z=-A-B+C. \tag{82b}$$

Because of the saddle points, there will be a negative jump in the derivative of $A_0(q)$ [saddle-point discontinuities (SPD)] at

$$q=2\cos^{-1}[(-\mu+B-C)/A] \tag{83}$$

for

$$B-C>\mu>-A+B-C, \tag{84}$$

and at

$$q=2\pi-2\cos^{-1}[(-\mu+B-C)/A] \tag{85}$$

for

$$\mu>B-C. \tag{86}$$

A similar behavior results from the saddle point (82b).

These considerations are borne out in detail by the shape of the computed $A_0(q)$ curves. The detailed shape is, of course, quite complicated and depends on the relative positions of the various special points. To illustrate the detailed shape of the curves, some computer curves of $A_0(q)$ of the orthorhombic structure in Table I are given in Figs. 3–5. Because of the limited accuracy of our numerical calculations the points of infinite slope (PIS) only show large slopes and the SPD's are not quite sharp, but this is almost certainly due to numerical inaccuracy. Figure 3 shows the results for $q=q_z$.

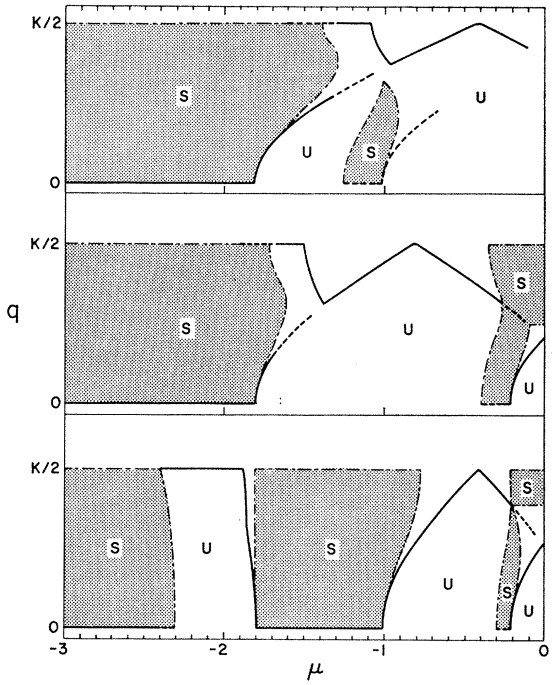

FIG. 9. Same as Fig. 6 for orthorombic band of Table I. From top to bottom the graphs are for q along [100], q along [010], and q along [100].

For $\mu=-2$, the function $A_0(q)$ is monotonic decreasing, with a large maximum of negative slope near

$$q=0.82\pi.$$

Equation (77) gives, for the negative PIS,

$$q=0.816\pi.$$

The first saddle point $(\pi, 0, 0)$ appears for $\mu=-1.8$. There is still a very large negative slope for $q\sim0.91\pi$, and $A_0(q)$ has a large negative slope near $q=0$ [as in Fig. 2(b)] due to the saddle point.

At $\mu=-1.6$, $A_0(q)$ increases from $q=0$ to the point of discontinuity (SPD)

$$q=0.34\pi,$$

while (83) gives, for the diameter of the neck,

$$0.354\pi.$$

For this value of μ, the large negative slope disappears ($\mu=-A-B$). Above this value of μ, a maximum appears at the zone boundary because $k_z{}^f>\frac{1}{2}\pi$.

[28] In all cases treated $A<B+C$. Otherwise hole sp would appear in the lower half band.

It can be seen that the point of infinite positive slope and the SPD coalesce for $\mu=-1$. At this point, the second saddle point at $(0, \pi, 0)$ also appears.

Above this point, the shape of $A_0(q)$ is complicated. The umklapp maximum on the zone boundary disappears because the SPD appears between the point of infinite positive slope and the zone boundary. The reflection of this behavior on the position of the maximum of $A_0(q)$ can also be seen in Fig. 9.

For $\mu<-1.8$, the maximum is at $q=0$. One then gets the spin-density waves due to the neck around the saddle point at $(\pi, 0, 0)$. At $\mu=-1.6$, a maximum begins to appear on the zone boundary because $k_z^f>\frac{1}{2}\pi$. These maxima disappear near $\mu=-1$ because the point of infinite positive slope crosses the SPD. The effect of the second sp at -1 is also clear from Fig. 3. It can be seen there how the maxima due to the sp disappear.

We will not discuss the other cases in any detail. The results shown come about in a very similar fashion but the details are, of course, different because of the different relative positions of the SPD and the PIS.

It is interesting to note the peculiar behavior near the saddle points. Approaching such a point from below, a positive PIS disappears for q along the axis of the sp, and above it $A_0(q)$ is dominated by transverse SPD's. As a result, the maximum of $A_0(q)$ is at $q\neq 0$ both above and below the sp, but at the sp it is at $q=0$.[29]

This is seen very clearly in all four structures investigated. For the cubic structure, this phenomenon occurs at the triply-degenerate sp at $\mu=-1$ (Fig. 6).

For the tetragonal structure I (Fig. 7) it occurs at the doubly degenerate sp at $\mu=-1.4$. At the second sp ($\mu=-0.2$) there is again a local maximum at $q=0$ for transverse q, but the dominant maximum is that due to the doubly degenerate sp at -1.4.

For the tetragonal structure II (Fig. 8) the dominant sp is the lower one at $\mu=-1.8$, which gives a cusp. The doubly degenerate sp at $q=-0.6$ only gives rise to a local maximum. Similarly, in the orthorhombic structure, the dominant sp is the lowest one at $\mu=-1.8$.

IV. STABILITY OF THE FERROMAGNETIC STATE

It seems reasonable to assume that the wave-vector-dependent susceptibility $A_0(q)$ describes the magnetic behavior of the itinerant electrons for small polarizations (i.e., small d), at least in so far as the HF approximation is valid. If U becomes large, so that the self-consistent solutions require a large d, this is certainly no longer true. In particular, it is to be expected that the band-structure-sensitive effects we discussed in Sec. III will be drastically modified when there is a considerable polarization of the electrons. We have therefore investigated the stability of the ferromagnetic state at finite moments.

[29] Unless $A_0(q)$ is dominated by some other regions.

As discussed in Sec. II (and Appendix B), a ferromagnetic state can be described by an arbitrary $\mathbf{q}$ and $\theta=0$. Because the physical state is independent of $\mathbf{q}$, all derivatives with respect to $\mathbf{q}$ vanish. In investigating the stability it is thus sufficient to check stability with respect to d and θ at $\theta=0$, treating $\mathbf{q}$ as a parameter.

In practice, there are two stages to the calculations. For a given band structure, n and U, one first determines the self-consistent ferromagnetic solutions. One then checks the stability of the solutions with respect to θ, i.e., the sign of

$$(d^2E/d\theta^2)_{\theta=0,d,\mathbf{q}}, \tag{87}$$

where d was determined in the first stage and $\mathbf{q}$ is a parameter.

The first stage is, of course, just the standard treatment of itinerant-electron magnetism. There are nevertheless a few points of interest related to the shape of the density of states. This will be discussed in Sec. IV A. The properties of the derivatives (87) will be discussed in Sec. IV B. Some numerical results are presented in Sec. IV C.

A. Self-Consistent Ferromagnetic States

The self-consistency condition (33) [Eq. (C1)] for a ferromagnetic state (e.g., $\theta=0$) is most conveniently written

$$2d=\int^{\mu+}\rho(\epsilon)\,d\epsilon-\int^{\mu-}\rho(\epsilon)\,d\epsilon, \tag{88}$$

with the subsidiary condition

$$2n=\int^{\mu+}\rho(\epsilon)\,d\epsilon-\int^{\mu-}\rho(\epsilon)\,d\epsilon, \tag{89}$$

where $\rho(\epsilon)$ is the density of states of the band, μ^+ and μ^- are the Fermi levels for up and down spin, respectively, measured from the bottom of the respective bands, and

$$n=\tfrac{1}{2}(n_\uparrow+n_\downarrow); \qquad d=\tfrac{1}{2}(n_\uparrow-n_\downarrow),$$

as in Eq. (31).

Up to a certain critical value of the band splitting $(2Ud)$, both bands are occupied and

$$\mu^+=\mu+Ud; \qquad \mu^-=\mu-Ud. \tag{90}$$

Above this value one has

$$\mu^+=\mu(2n); \qquad \mu^-=0, \tag{91}$$

for $n<\frac{1}{2}$, where

$$2n=\int^{\mu(2n)}\rho(\epsilon)\,d\epsilon, \tag{92}$$

and for $n>\frac{1}{2}$

$$\mu^+=E_{\max}; \qquad \mu^-=\mu(2n-1), \tag{93}$$

where $E_{\max}$ is the top of the band, and

$$2n-1=\int^{\mu(2n-1)}\rho(\epsilon)d\epsilon. \tag{94}$$

Formally eliminating μ between Eqs. (88) and (89), one can write

$$d=F(Ud), \tag{95}$$

where $F(x)$ is a monotonic nondecreasing function of its argument which is constant above the critical value of x discussed above (see, e.g., Figs. 10 and 11). Self-consistent solutions of (95) for given U are given by the simultaneous solutions of

$$d=F(x), \tag{96a}$$

and

$$d=x/U. \tag{96b}$$

The nature of these solutions is determined by the shape of $F(x)$.

When $F(x)$ is convex for all x,

$$d^2F(x)/dx^2\leq 0, \tag{97}$$

it is dominated by the initial slope. This is illustrated in Fig. 10.

The paramagnetic solution ($d=0$) is stable for

$$U<U_c, \tag{98}$$

and a magnetic solution appears when

$$U>U_c, \tag{99}$$

where

$$1/U_c=(dF/dx)_{x=0}=\rho(\mu_0), \tag{100}$$

and $\rho(\mu_0)$ is the density of states at the paramagnetic Fermi level.

A very different behavior appears when there are concave regions where

$$d^2F/dx^2>0. \tag{101}$$

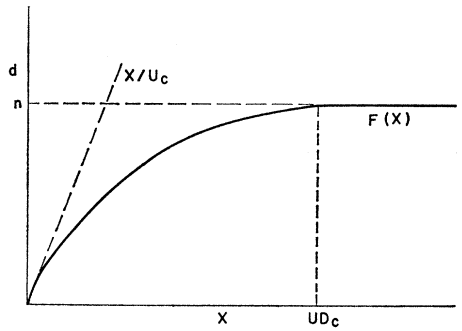

FIG. 10. Schematic description of graphic solution of self-consistency equations for band magnetism (96), when $d^2F/dx^2<0$ everywhere. Self-consistent magnetic solutions are possibly only for $U>U_c$, where $1/U_c$ is the initial slope of $F(x)$.

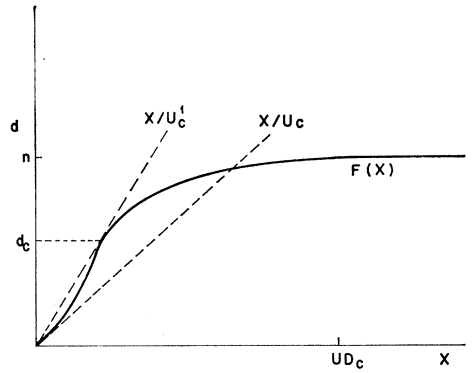

FIG. 11. Same as Fig. 10 when $d^2F/dx^2>0$ for $x<U_{c_1}d_c$. No stable solutions are possible with $d<d_c$.

This was first noted by Shimizu,[30] and by Wohlfarth and Rhodes.[31]

If there is one such region, Eq. (95) can have three solutions (Fig. 11), or even four. Moreover, there can be self-consistent solutions for

$$U<\rho(\mu_0)^{-1}, \tag{102}$$

as in Fig. 11. This leads to a discontinuous dependence of the moment d on U. There are no stable magnetic solutions with

$$d<d_c, \tag{103}$$

so that a finite magnetic moment ($d>d_c$) appears above a certain $U(>U_{c_1})$ while below it the paramagnetic state is stable. A necessary and sufficient condition for this type of anomaly is that the inequality [Eq. (101)] should hold for some x. Now, from Eqs. (88) and (89),

$$\frac{d^2F}{dx^2}=C\left(\frac{d\rho(\mu^+)}{dt}\Big/\rho(\mu^+)^3-\frac{d\rho(\mu^-)}{dt}\Big/\rho(\mu^-)^3\right), \tag{104}$$

where

$$C=4\{\rho(\mu^+)\,\rho(\mu^-)/[\rho(\mu^+)+\rho(\mu^-)]\}^3. \tag{105}$$

It is easy to see that the situation in Eq. (101) can never occur for free-electron dispersions ($\epsilon_k\sim k^2$).

Shimizu[30] discussed the situations near a minimum in the density-of-states curve where $d\rho(\mu^-)/d\epsilon<0$ while $d\rho(\mu^+)/d\epsilon>0$. For example, the cubic band structure of Table I has a (very shallow) minimum for $\mu=0$. As a result, this type of instability is observed when

$$0<\mu^+<1.0; \qquad 1<\mu^-<0.$$

A second possibility is that $\rho(\mu^+)$ might become small e.g., near maxima in the band structure.

---

[30] M. Shimizu and A. Katsuki, Phys. Letters **8**, 7 (1964); M. Shimizu, Proc. Phys. Soc. (London) **84**, 397 (1964); **86**, 147 (1965).

[31] E. P. Wohlfarth and P. Rhodes, Phil. Mag. **7**, 1817 (1962).

A third situation is

$$d\rho(\mu^+)/d\epsilon \gg d\rho(\mu^-)/d\epsilon. \tag{106}$$

It is well known that this can occur below a saddle point where $d\rho/d\epsilon$ diverges while ρ remains finite. This should be a fairly common phenomenon and occurs below all saddle points in our calculations.

It is of interest to note[31] that the inequality (97) also leads to peculiarities in the behavior of the magnetization at finite magnetic fields which might be observable in suitable cases.

In our numerical calculations it was found in all cases that the metastable solutions of Eq. (96) were also unstable with respect to spirals. In fact, we never found a case where there was a stable ferromagnetic solution which did not have $U\rho(\mu_0)>1$. We believe this is probably true, in general, at least for cases where Eq. (101) occurs because of saddle points. Even in the simple bands that we investigated, it would, however, require a very careful analysis to be sure. Such a calculation was not carried out.

B. Stability with Respect to θ

The relevant derivatives are given in Appendix C. Obviously,

$$(dE/d\theta)_{\theta=0}=(d^2E/d(d)d\theta)_{\theta=0}\equiv 0,$$

because $\sin\theta=0$. One is therefore left with

$$K(d,q)=\left(\frac{d^2E}{d\theta^2}\right)_{\substack{d,\mathbf{q}\\ \theta=0}}=-\int^{\epsilon_k<\mu^+} d\mathbf{k}\,\frac{Ud(\epsilon_k-\epsilon_{k+q})}{2Ud-(\epsilon_k-\epsilon_{k+q})} -\int^{\epsilon_k<\mu^-} d\mathbf{k}\,\frac{Ud(\epsilon_k-\epsilon_{k+q})}{2Ud+(\epsilon_k-\epsilon_{k+q})}, \tag{107}$$

which can be obtained from Eqs. (C7) and (C8).

It is obvious from the form of the integrals (107) that

$$K(0,q)=K(d,0)\equiv 0. \tag{108}$$

Further, it can be seen that there is a considerable amount of cancellation between the two integrals. The contribution to the first integral from the region

$$\epsilon_k<\mu^+; \qquad \epsilon_{k+q}<\mu^-, \tag{109a}$$

exactly cancels that from the region

$$\epsilon_k<\mu^-; \qquad \epsilon_{k+q}<\mu^+, \tag{109b}$$

in the second integral in (107).

To discuss the analytic structure of $K(d,\mathbf{q})$, it is convenient to rewrite the integrals in the form

$$K(d,\mathbf{q})=2Ud^2\,|\,1-U[F^+(\mathbf{q})+F^-(\mathbf{q})]\,|, \tag{110}$$

where

$$F^+(\mathbf{q})=\int^{\epsilon_k<\mu^+} d\mathbf{k}(2Ud-\epsilon_k+\epsilon_{k+q})^{-1}, \tag{111a}$$

and

$$F^-(\mathbf{q})=-\int^{\epsilon_k<\mu^-} d\mathbf{k}(2Ud+\epsilon_k-\epsilon_{k+q})^{-1}. \tag{111b}$$

It is easy to see that outside the regions of cancellation [Eq. (109)] the integrals in (111a) and (111b) are positive (because $\mu^+-\mu^-\geq 2Ud$). As a result, the quantity in brackets in Eq. (110) (F^++F^-) is positive, and the stability condition

$$K(d,\mathbf{q})\geq 0 \tag{112}$$

is very similar to Eq. (40).

The integrals of Eq. (111) are very similar to those discussed previously [Eq. (41)], and show the same types of singularities. It is of some interest to discuss this in more detail.

1. The Limit of Small q

For $\mathbf{q}$ along any direction

$$\boldsymbol{\alpha}=\mathbf{q}/q, \tag{113}$$

one can expand

$$\epsilon_{k+q}-\epsilon_k=q\,\boldsymbol{\alpha}\cdot\nabla_k\epsilon_k+\tfrac{1}{2}q^2\boldsymbol{\alpha}\cdot(\nabla_k\cdot\nabla_k\epsilon_k)\cdot\boldsymbol{\alpha}. \tag{114}$$

It follows that

$$F^+(\mathbf{q})=(2Ud)^{-1}\int^{\epsilon_k<\mu^+} d\mathbf{k}\left[1-\frac{q}{2Ud}\,\boldsymbol{\alpha}\cdot\nabla_k\epsilon_k -\frac{q^2}{4Ud}\,\boldsymbol{\alpha}\cdot(\nabla\cdot\nabla\epsilon_k)\cdot\boldsymbol{\alpha}+\left(\frac{q}{2Ud}\right)^2(\boldsymbol{\alpha}\cdot\nabla\epsilon_k)^2\right], \tag{115a}$$

$$F^-(\mathbf{q})=(2Ud)^{-1}\int^{\epsilon_k<\mu^-} d\mathbf{k}\left[1+\frac{q}{2Ud}\,\boldsymbol{\alpha}\cdot\nabla\epsilon_k +\frac{q^2}{4Ud}\,\boldsymbol{\alpha}\cdot(\nabla\cdot\nabla\epsilon_k)\cdot\boldsymbol{\alpha}+\left(\frac{q}{2Ud}\right)^2(\boldsymbol{\alpha}\cdot\nabla\epsilon_k)^2\right], \tag{115b}$$

and therefore

$$K(d,q)=\tfrac{1}{4}q^2\left\{\int^{\epsilon_k<\mu^+} d\mathbf{k}[\boldsymbol{\alpha}\cdot(\nabla\cdot\nabla\epsilon\mathbf{k})\cdot\boldsymbol{\alpha}-(\boldsymbol{\alpha}\cdot\nabla\epsilon_k)^2/Ud] +\int^{\epsilon_k<\mu^-} d\mathbf{k}[\boldsymbol{\alpha}\cdot(\nabla\cdot\nabla\epsilon_k)\cdot\boldsymbol{\alpha}+(\boldsymbol{\alpha}\cdot\nabla\epsilon_k)^2/Ud]\right\}. \tag{116}$$

In deriving (116), we have used the fact that the constants in the integrand (115) cancel the constant (1) in (111), and the integrals linear in q vanish because of time-reversal symmetry (i.e., $\nabla\epsilon_k=-\nabla\epsilon_{-k}$).

It is thus seen that $K(d,\mathbf{q})$ vanishes and has an extremum at $\mathbf{q}=0$.

2. Free Electrons

As in Sec. III A, it is instructive to investigate the behavior of $K(d,\mathbf{q})$ for free electrons when the integrals (111) can be evaluated explicitly.

Using

$$\epsilon_k = k^2; \qquad \mu^{\pm} = (k_f^{\pm})^2,$$

one finds a result similar to (42), namely,

$$K_{\text{free}}(d, \mathbf{q})/2Ud^2 = 1 + (U/2q) \times [\phi(k_f^+, Q^+) + \phi(k_f^-, Q^-)], \quad (117)$$

where

$$\phi(k, Q) = (k^2 - Q^2) \ln | (k+Q)/(k-Q) | + 2kQ, \quad (118)$$

and

$$Q^{\pm} = \tfrac{1}{2}q \pm Ud/q. \quad (119)$$

Obviously, ϕ has a logarithmic singularity when

$$k = Q. \quad (120)$$

As a function of q there are, in fact, two such singularities for

$$q = k_f^+ \pm k_f^-. \quad (121)$$

It can, however, be seen that the lower one ($q = k_f^+ - k_f^-$) cancels between the two ϕ in square brackets in (117).

An additional feature which should be mentioned is the behavior for large U. When Ud is large enough,

$$\phi(k^-, Q^-) = 0,$$

because

$$k^- = 0.$$

In this range, there are also no logarithmic singularities in $\phi(k^+, Q^+)$ because

$$Q^+ > (2Ud)^{1/2} \quad (122)$$

from (119), and is therefore never small enough to fulfill Eq. (120).

3. *General Features of $K(d,\mathbf{q})$*

It is possible to carry out a detailed analysis of the properties of $K(d, \mathbf{q})$ analogous to our analysis of $A_0(\mathbf{q})$ in Sec. III. In particular, the effect of umklapp processes and saddle points can be analyzed as in Secs. III B and III C. The algebra does, however, become very cumbersome and uninteresting. Apparently there are no really new analytic properties. This also seems plausible in view of the great formal similarity between the integrals (111) and $A_0(q)$ [Eq. (42)]. The constant $2Ud$ appears in the denominators simply because the up- and down-spin bands are split by this amount.

The only really important effects are those due to the different positions of the Fermi surface in the spin-up band μ^+ and in the spin-down band μ^-.

Consider first the small splitting situation

$$\mu^- \neq 0.$$

It was shown in Sec. IV B2 that the (positive) logarithmic divergence in the derivative of $K(d, \mathbf{q})$ appears at

$$\mathbf{q} = \mathbf{k}_f^+ + \mathbf{k}_f^- \quad (123a)$$

instead of $2\mathbf{k}_f$. When

$$\mathbf{k}_f^+ + \mathbf{k}_f^- > \tfrac{1}{2}\mathbf{K},$$

this is replaced by a negative divergence at

$$\mathbf{K} - \mathbf{q} = \mathbf{k}_f^+ + \mathbf{k}_f^-. \quad (123b)$$

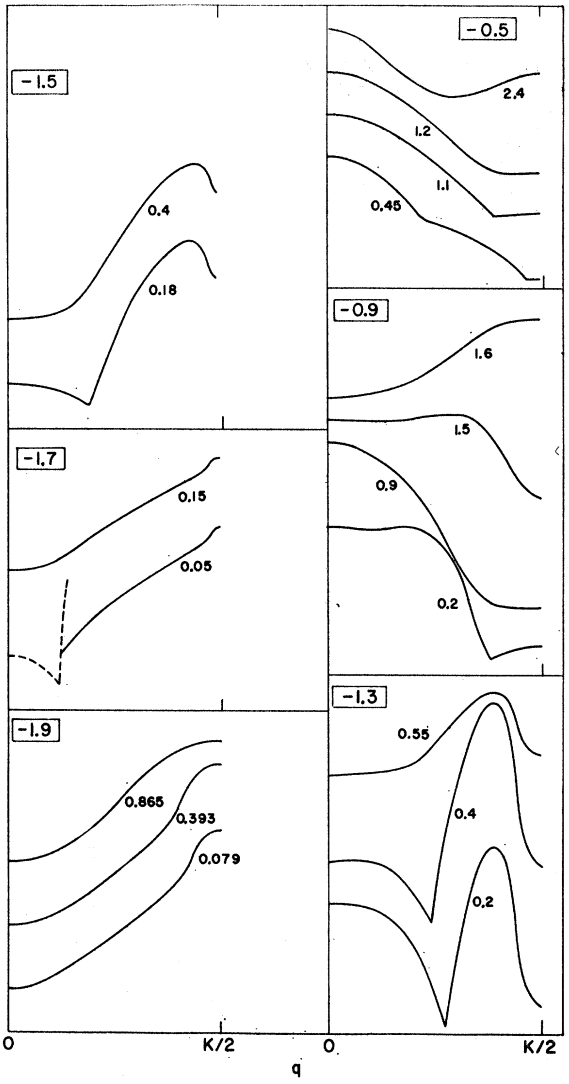

FIG. 12. Some typical curves of the transverse stability integral $K(d, \mathbf{q})$ for $\mathbf{q}$ along the [001] direction in the orthorombic band structure of Table II. For each family of constant n curves the position of the corresponding paramagnetic Fermi level is given in a frame. The band-splitting parameter Ud is indicated near each curve. Further details on the ferromagnetic states are given in Table II. As in Figs. 3–5, the horizontal scale gives q up to $\frac{1}{2}K$. The vertical scale is different and shifted for each curve. As $K(d, 0) \equiv 0$, the zero for each curve can be seen from its value at $q = 0$. In the curve for $\mu = -1.7$ and $Ud = 0.05$ the lower (dashed) portion of the curve is drawn on a larger scale than the rest of the curve to show the effect of the sp. Note the discontinuities in the derivatives when there are two necks and the role of the negative slopes due to umklapp processes. Obviously, the ferromagnetic state is stable when K is positive and unstable when it is negative.

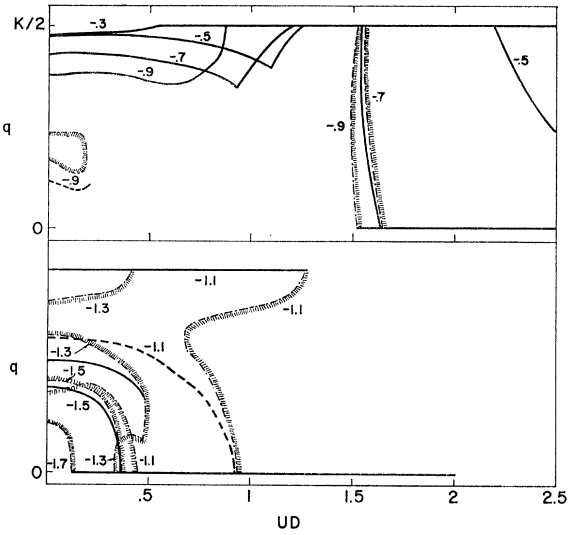

FIG. 13. Curves indicating the regions for which $K(d, \mathbf{q})$ is negative and the values of q for which the negative value has a minimum for $\mathbf{q}$ along [001] and the orthorombic band structure of Table II. The vertical scale gives $\mathbf{q}$ and the horizontal scale gives the band-splitting parameter Ud. The boundaries of the negative-K region are shaded on the outside and the position of the minimum is indicated by solid curves (dashed for secondary minima). When the position of the minimum is not indicated it is either at $q=0$ ($K>0$) or on the boundary, depending on the stability region. For each curve, the value of the paramagnetic Fermi level is indicated. Additional details on the ferromagnetic state are given in Table III.

The effect of saddle points is also similar to that discussed in Sec. III C. There is a (positive) discontinuity in the derivative of $K(d, \mathbf{q})$ when $\mathbf{q}$ is equal to the sum of the radii of the up- and down-spin necks. The discontinuity disappears when μ^- drops below the saddle point. Some illustrations are given in Fig. 12 and will be discussed in Sec. IV C.

4. *Limit of Large Band Splitting*

The large band splitting limit is much less sensitive to detailed band-structure effects. It should therefore be discussed separately. It is possible to expand our expression for the HF energy (29) directly in this limit. We will, however, restrict ourselves to the large Ud limit of $K(d, \mathbf{q})$.

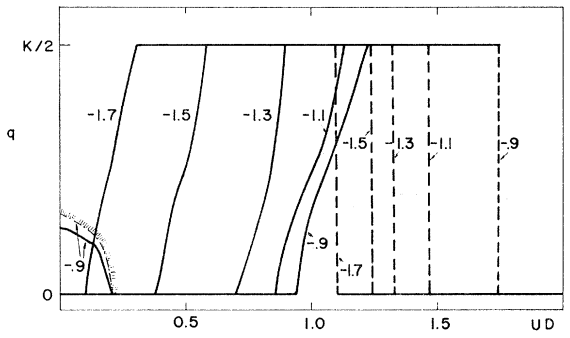

FIG. 14. Same as Fig. 13 for Z along [100].

There are two types of situations. For intermediate Ud one has

$$2Ud>\mu(2n) \tag{124}$$

and therefore from (91),

$$\mu^-=0; \qquad \mu^+-\mu^->2Ud. \tag{125}$$

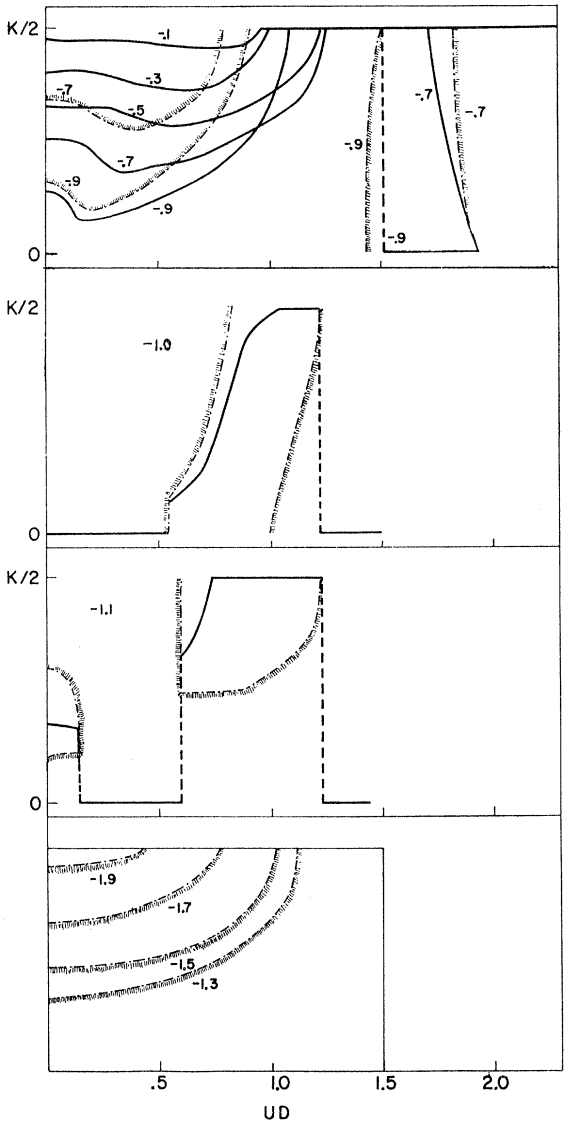

FIG. 15. Same as Fig. 13 for cubic band structure and $\mathbf{q}$ along [100].

As a result, the denominators in Eq. (112) remain finite for all $\mathbf{k}$, and there are no logarithmic divergences in the derivative of $K(d, \mathbf{q})$. If Ud is not too large, one does, however, observe the remains of the singularity, and the derivative is large for

$$q\sim k_f^+. \tag{126}$$

This effect was noted for example in the free-electron case (Sec. IV B2).

TABLE II. Values of the paramagnetic Fermi level μ, number of electrons $[n=\frac{1}{2}(n\uparrow+n\downarrow)]$, the band splitting parameter Ud, the interaction U, the population difference $[d=\frac{1}{2}(n\uparrow-n\downarrow)]$, and the positions of the spin-up Fermi level $\epsilon_f{}^+$ and spin-down Fermi level $\epsilon_f{}^-$ for the orthorhombic band structure of Table I. Only the values at the points for which $K(d, \mathbf{q})$ is shown in Fig. 12 are given. Energy units are $\frac{1}{6}$ of band width.

μ	$n(\mu)$	Ud	d	U	$E_f{}^+$	$E_f{}^-$
−1.9	0.076	0.079	0.010	7.744	−1.825	−1.983
		0.393	0.048	8.226	−1.593	−2.379
		0.865	0.076	11.308	−1.428	−3.000
−1.7	0.106	0.050	0.008	6.132	−1.650	−1.750
		0.150	0.024	6.223	−1.556	−1.856
−1.5	0.140	0.180	0.031	5.737	−1.326	−1.686
		0.400	0.068	5.856	−1.136	−1.936
−1.3	0.176	0.200	0.038	5.296	−1.109	−1.509
		0.400	0.076	5.254	−0.938	−1.738
		0.550	0.103	5.331	−0.826	−1.926
−0.9	0.262	0.200	0.047	4.259	−0.706	−1.106
		0.900	0.192	4.683	−0.156	−1.956
		1.500	0.261	5.756	+0.075	−2.925
		1.600	0.262	6.114	+0.079	−3.000
−0.5	0.360	0.450	0.117	3.848	−0.077	−0.977
		1.100	0.264	4.172	+0.439	−1.761
		1.200	0.282	4.250	+0.511	−1.889
		2.400	0.360	6.661	+0.826	−3.000

Finally, one can consider the case of very large band splitting. This always leads to a stable ferromagnetic state, i.e., to

$$K(d, \mathbf{q})>0. \tag{127}$$

Expanding (110) gives

$$K(d, \mathbf{q})=\frac{1}{2}\int^{\epsilon_k<\mu(2n)}(\epsilon_{k+q}-\epsilon_k)\,d\mathbf{k}-(4Un)^{-1}\times\int^{\epsilon_k<\mu(2n)}(\epsilon_k-\epsilon_{k+q})^2 d\mathbf{k}+\cdots. \tag{128}$$

The first term on the right side of (128) is positive and the second term is negative. For sufficiently large U the first (linear) term dominates, so that $K(d, \mathbf{q})$ becomes positive.

The only exception is the insulating case

$$2n=1 \tag{129}$$

when all states $\mathbf{k}$ are occupied and the first integral on the right side vanishes. As a result, it becomes increasingly difficult to reach this large-splitting ferromagnetism as $2n$ approaches one. This can be seen in Figs. 13–15.

C. Illustrative Calculations of $K(d, \mathbf{q})$

We have calculated $K(d, \mathbf{q})$ numerically for the tight-binding band structures of Table I, and in each case a considerable number of suitably chosen values of the band splitting Ud. Most of the conclusions from these calculations were discussed in Secs. IV A and B. Some of the results are presented in Figs. 12–15.

TABLE III. Important values of Ud for the orthorhombic band structure of Table I for different positions of the paramagnetic Fermi surface μ. The values relevant to the curves in Figs. 12 and 14 are given. For clarity, we also give n for each μ and the values of U and d at each point. Energy units are $\frac{1}{6}$ of band width.

			$\epsilon_f{}^-=-3$		$\epsilon_f{}^-=-1.8$			$\epsilon_f{}^-=-1.0$		
μ	$n(\mu)$	$U_c=\rho(\mu)^{-1}$	Ud	U	Ud	U	d	Ud	U	d
−1.9	0.076	7.745	0.785	10.20						
−1.7	0.106	6.132	0.938	8.80	0.09	6.131	0.015			
−1.5	0.140	5.739	1.089	7.77	0.29	5.737	0.0505			
−1.3	0.176	5.304	1.235	7.02	0.45	5.251	0.0857			
−1.1	0.216	4.771	1.385	6.41	0.61	4.88	0.1250			
−0.9	0.262	4.181	1.540	5.90	0.79	4.595	0.172	0.09	4.180	0.0215
−0.7	0.310	4.064	1.713	5.52	0.95	4.327	0.219	0.29	4.052	0.0716
−0.5	0.360	3.910	1.913	5.32	1.13	4.192	0.270	0.47	3.848	0.122
−0.3	0.413	3.680	2.156	5.20	1.35	4.172	0.324	0.65	3.722	0.175
−0.1	0.470	3.381	2.523	5.35	1.63	4.277	0.381	0.89	3.777	0.236

TABLE IV. Same as Table III for cubic band.

			$\epsilon_f^-=-3$		$\epsilon_f^-=-1$		
μ	n	U_c	Ud	U	Ud	U	d
−1.9	0.0669	9.485	0.804	12.01			
−1.7	0.0899	8.024	0.929	10.6			
−1.5	0.117	6.777	1.035	8.85			
−1.3	0.149	5.645	1.148	7.66			
−1.1	0.189	4.487	1.286	6.82			
−1.0	0.213		1.372	6.45			
−0.9	0.242	3.465	1.473	6.08	0.10	3.47	0.029
−0.7	0.300	3.481	1.674	5.58	0.30	3.48	0.086
−0.5	0.357	3.493	1.875	5.25	0.50	3.49	0.143
−0.3	0.414	3.500	2.092	5.05	0.70	3.49	0.201
−0.1	0.471	3.504	2.499	5.28	0.90	3.49	0.258

Figure 12 shows some typical curves of $K(d, \mathbf{q})$ as a function of $\mathbf{q}$. For convenience, the curves are indicated by the position of the paramagnetic Fermi level μ and by the band-splitting parameter Ud. The number of electrons $n(\mu)$, and, for each Ud, the values of U and d, and the positions of the Fermi level for up spins ϵ_f^+ and for down spin ϵ_f^- are given in Table II.

The curves given are all for $\mathbf{q}$ along the z axis of the orthorhombic structure in Table I. The band structure was discussed in Sec. III D.

For $\mu=-1.9$, we are still below the first saddle point. $K(d, \mathbf{q})$ is positive and monotonic increasing for all $\mathbf{q}$ and Ud. For small Ud ($Ud=0.079$ and 0.393) one observes the free-electron positive logarithmic singularity in the derivative (point of PIS) when

$$\mathbf{q}=\mathbf{k}_f^+ + \mathbf{k}_f^- \tag{130}$$

along this direction (see Sec. IV B2). For large Ud (0.865) the lower band is empty, i.e.,

$$\epsilon_f^-=-3.0,$$

and there is no point of PIS. Except for this, the curves remain similar.

For $\mu=-1.7$, there is a small neck due to the saddle point at -1.8 (see Sec. III D). As a result, K becomes negative,

$$(d^2K(d, \mathbf{q})/dq^2)_{\mathbf{q}=0}<0, \tag{131}$$

and has a positive discontinuity in the derivative (SPD) when

$$\mathbf{q}=\mathbf{s}^+ + \mathbf{s}^-. \tag{132}$$

In (132), s^+ is the radius of the spin-up neck along z, and s^- is the radius of the spin-down neck. This can be seen in the curve for $Ud=0.05$. When

$$\epsilon_f^-<-1.8,$$

the spin-down neck disappears. This can be seen, for example, for $Ud=0.15$ (see also Table II). There is no SPD and the effect of the sp disappears. In Fig. 13, on the curves for $\mu=-1.7$, it can be seen that both the negative maximum in K (at the point 130) and the region where K is negative disappears abruptly when

$$Ud\approx 0.1.$$

In fact,

$$\epsilon_f^-=-1.8$$

for $Ud=0.09$ (see Table III).

For this value of μ^- and direction of $\mathbf{q}$, one always has

$$\mathbf{k}_f^+ + \mathbf{k}_f^- < \tfrac{1}{2}\mathbf{K}. \tag{133}$$

One, therefore, observes the positive PIS in $K(d, \mathbf{q})$ for the $\mathbf{q}$ of 130.

When $\mu=-1.5$, the effect of the sp is more pronounced. There is also a minimum in K at the zone boundary due to the negative PIS for

$$\mathbf{K}-\mathbf{q}=\mathbf{k}_f^+ + \mathbf{k}_f^-.$$

Both effects become stronger for $\mu=-1.3$. In each of the two lower curves $UD=0.2$ and 0.4 there are two separate negative regions in K. One for low q due to the sp and a second region near the zone boundary due to the PIS. It is interesting to compare these curves with Table III and the relevant curves in Fig. 13. It can be seen that the lower negative region in K disappears abruptly when the neck in the spin-down Fermi surface disappears ($Ud\approx 0.45$). On the other hand, the disappearance of the negative region at the zone boundary is rather accidental. There is still a negative PIS for larger Ud but the resulting minimum in K is positive (see curve for $Ud=0.55$ in Fig. 12).

The cases of $\mu=0.9$ and $\mu=-0.5$ can be analyzed in a similar fashion. Note that the sp at $\mu=-1$ still has some effect when $\epsilon_f^-<-1.0$. Even clearer is the effect of the sp at -1.8, which is evident for quite large Ud when ϵ_f^- is quite low. Note also, that the negative PIS disappears when $\epsilon_f^+>-0.2$, so that the spin-up Fermi surface touches the zone boundary along this direction. For $\mu=-0.9$ this point can be seen for $Ud=0.2$ but it disappears for $Ud=0.9$ (compare Table II).

In Figs. 13–15, the regions for which K is negative and for each region, the value of q for which it is most negative, are shown as a function of the band-splitting parameter Ud for a number of different positions of the

Fermi surface. As mentioned above, Fig. 13 is for the orthorhombic structure of Table I and $q=q_x$. Figure 14 gives some data for this structure and $q=q_z$. Figure 15 gives results for a cubic band. The results for a cubic band are closely related to the results of Penn.[7] Some relevant data on the band structure are given in Tables II–IV.

Results for the two tetragonal band structures of Table I and for the y direction in the orthorhombic structure were also obtained. They are, however, similar to those presented and do not seem to add any new insight.

ACKNOWLEDGMENT

We would like to thank Dr. D. Newman of the Belfer Graduate School of Science, Yeshiva University, for the proof in Appendix D.

APPENDIX A: RIGOROUS DEFINITION OF LOCAL DIRECTION OF QUANTIZATION

We want to prove that for a general many-body wave function, it, is always possible to find a direction z_α for the local moment, i.e., such that the magnitude of the moment μ is given by its expectation value along that direction. If the state has a local moment, then in an arbitrary representation not all of $\langle S^z\rangle$, $\langle S^+\rangle$, and $\langle S^-\rangle$ can be zero. We can then find a transformation such that

$$\mu=\langle S^z\rangle=\tfrac{1}{2}\langle n_{\alpha\uparrow}-n_{\alpha\downarrow}\rangle, \tag{A1}$$

$$\langle S^+\rangle=\langle d_{\alpha\uparrow}{}^\dagger d_{\alpha\downarrow}\rangle=0, \tag{A2}$$

$$\langle S^-\rangle=\langle d_{\alpha\downarrow}{}^\dagger d_{\alpha\uparrow}\rangle=0, \tag{A3}$$

where the $d_{\alpha\sigma}$ are defined for spin quantization along z_α.

This is sufficient to prove that (21) is indeed the complete HF decoupling when the direction z_α is chosen properly because the expectation values in all other forms of decoupling vanish.

We believe the proof is also of interest because it shows that the introduction of a local direction of quantization can be given an exact formal meaning.

A general N-particle wave function in the Hilbert space spanned by the Wannier state $w_{\alpha\sigma}$ (with a creation operator $c_{\alpha\sigma}{}^\dagger$) can always be written in second quantization

$$\Psi=\Phi_0+\Phi_\downarrow c_{\alpha\downarrow}{}^\dagger+\Phi_\uparrow c_{\alpha\uparrow}{}^\dagger+\Phi_{\uparrow\downarrow}c_{\alpha\uparrow}{}^\dagger c_{\alpha\downarrow}{}^\dagger, \tag{A4}$$

where Φ_0 is an N-particle wave function in which w_α is unoccupied, $\Phi_\uparrow$ and $\Phi_\downarrow$ are $(N-1)$-particle wave functions in which w_α is unoccupied, and $\Phi_{\uparrow\downarrow}$ is an $(N-2)$-particle wave function of the same type.

From (A1)–(A3) for a general direction of quantization

$$\langle S_\alpha{}^z\rangle=\tfrac{1}{2}(|\,\Phi_\uparrow\,|^2-|\,\Phi_\downarrow\,|^2)=\mu_z, \tag{A5}$$

$$\langle S_\alpha{}^+\rangle=\langle\Phi_\uparrow\,|\,\Phi_\downarrow\rangle=Ae^{i\phi}, \tag{A6}$$

$$\langle S_\alpha{}^-\rangle=\langle\Phi_\downarrow\,|\,\Phi_\uparrow\rangle=Ae^{-i\phi}, \tag{A7}$$

where A and ϕ are real numbers; Φ_0 and $\Phi_{\uparrow\downarrow}$ do not contribute.

Using the transformation (10) it is easy to see that (A2) and (A3) are obeyed if one chooses

$$\phi_\alpha=-\phi, \tag{A8}$$

$$\tan\theta=A/\mu_z, \tag{A9}$$

which is, of course, identical with the single-electron result.

When the many-particle wave function is an eigenfunction of $S_{\rm tot}{}^2=\sum_\alpha S_\alpha{}^2$ with well-defined $M_{\rm tot}{}^2$ it is of course trivial to show that $\langle S_\alpha{}^+\rangle=\langle S_\alpha{}^-\rangle=0$ [Eqs. (A6) and (A7)] because $\Phi_\uparrow$ and $\Phi_\downarrow$ have different spin. This is, however, not a valid assumption in the present context, and our proof is much more general.

APPENDIX B: SOME PROPERTIES OF E(d, q, ϑ)

The simplest properties are those resulting from the time-reversal symmetry of the Hamiltonian and are rather trivial, namely,

$$E(d)=E(-d), \tag{B1}$$

$$E(\mathbf{q})=E(-\mathbf{q}), \tag{B2}$$

where (B2) follows from $\epsilon_{\rm k}=\epsilon_{\rm k}$.

Less obvious are the following: For $d=0$, the $G_{\rm kk}$ always describe the same paramagnetic state, so that the choice of $\mathbf{q}$ and θ only relabels the poles. It follows that

$$E(d,\mathbf{q},\theta)_{d=0}=\text{const}, \tag{B3}$$

independent of $\mathbf{q}$ and θ. This is automatically true and is not a subsidiary condition.

Further, $\mathbf{q}=0$ is always a ferromagnetic state whatever θ. Similarly, $\theta=0$ is ferromagnetic and is independent of $\mathbf{q}$. Thus,

$$E(d,\mathbf{q},\theta)\,|_{\mathbf{q}=0}=E(d,\mathbf{q},\theta)\,|_{\theta=0}=E(d)\,|_{\rm ferromag.} \tag{B4}$$

Obviously, (B1)–(B4) follow algebraically from the definition of $E(d,\mathbf{q},\theta)$ [Eq. (24)].

APPENDIX C: EXTREMUM CONDITIONS OF THE INTERNAL ENERGY

The derivatives of the energy (37) with the subsidiary condition (38) are

$$\left(\frac{\partial E}{\partial d}\right)_{\mathbf{q},\theta}=2Ud-U\int^\mu\frac{\partial L}{\partial Ud}\,2\,\mathrm{Im}[G^-(\epsilon)-G^+(\epsilon)]d\epsilon, \tag{C1}$$

which is identical with Eq. (33).

$$\left(\frac{\partial E}{\partial\theta}\right)_{d,\mathbf{q}}=-\sin\theta\int^\mu\frac{\partial L}{\partial\cos\theta}\,2\,\mathrm{Im}[G^-(\epsilon)-G^+(\epsilon)]d\epsilon, \tag{C2}$$

$$(\partial^2E/\partial d^2)_{\mathbf{q},\theta}=2U^2[1/U-A-B+C], \tag{C3}$$

where

$$A=\frac{1}{2}\int^{\mu}\frac{\partial^2 L}{\partial(Ud)^2}\,2\ \mathrm{Im}\mid G^-(\epsilon)-G^+(\epsilon)\mid d\epsilon, \quad \text{(C4)}$$

$$B=\tfrac{1}{2}(\partial L/\partial Ud)^2\,2\ \mathrm{Im}[G^+(\mu)+G^-(\mu)], \quad \text{(C5)}$$

$$C=\frac{1}{2}\frac{\{[\partial L/\partial(Ud)]\,2\ \mathrm{Im}[G^-(\mu)-G^+(\mu)]\}^2}{2\ \mathrm{Im}[G^-(\mu)+G^+(\mu)]}. \quad \text{(C6)}$$

Further,

$$(\partial^2 E/\partial\theta\partial d)_{\mathrm{q}}=-\sin\theta(D+F-H), \quad \text{(C7)}$$

where

$$D=U\int^{\mu}\frac{\partial^2 L}{\mu(Ud)\partial\cos\theta}2\ \mathrm{Im}[G^-(\epsilon)-G^+(\epsilon)]d\epsilon, \quad \text{(C8)}$$

$$F=U\frac{\partial L}{\partial\cos\theta}\frac{\partial L}{\partial Ud}\,2\ \mathrm{Im}[G^-(\mu)+G^+(\mu)], \quad \text{(C9)}$$

$$H=U\frac{\{(\partial L/\partial\cos\theta)\ 2\ \mathrm{Im}[G^-(\mu)-G^+(\mu)]\}\cdot\{(\partial L/\partial Ud)\ 2\ \mathrm{Im}[G^-(\mu)-G^+(\mu)]\}}{2\ \mathrm{Im}[G^-(\mu)+G^+(\mu)]}. \quad \text{(C10)}$$

Finally,

$$(\partial^2 E/\partial\theta^2)_{d,\mathrm{q}}=-\cos\theta I+\sin^2\theta(J+K-L), \quad \text{(C11)}$$

$$I=\int^{\mu}\frac{\partial L}{\partial\cos\theta}\,2\ \mathrm{Im}[G^-(\epsilon)-G^+(\epsilon)]d\epsilon, \quad \text{(C12)}$$

$$J=\int^{\mu}\frac{\partial^2 L}{\partial\cos\theta^2}\,2\ \mathrm{Im}[G^-(\epsilon)-G^+(\epsilon)]d\epsilon, \quad \text{(C13)}$$

$$K=(\partial L/\partial\cos\theta)^2\,2\ \mathrm{Im}[G^-(\mu)+G^+(\mu)], \quad \text{(C14)}$$

$$L=\frac{\{(\partial L/\partial\cos\theta)\ 2\ \mathrm{Im}[G^-(\mu)-G^+(\mu)]\}^2}{2\ \mathrm{Im}[G^-(\mu)+G^+(\mu)]}. \quad \text{(C15)}$$

The derivative of L in the above equations are

$$\partial L/\partial Ud=(Ud-D\cos\theta)/L, \quad \text{(C16)}$$

$$\partial^2 L/\partial U_d{}^2=(D^2\sin^2\theta)/L^3, \quad \text{(C17)}$$

$$\partial L/\partial\cos\theta=-DUd/L,$$

$$\partial^2 L/\partial\cos\theta^2=-D^2(Ud)^2/L^3. \quad \text{(C18)}$$

In deriving these equations, it is useful to notice that

$$\frac{\partial G^{\pm}}{\partial(Ud)}=\frac{\partial L}{\partial Ud}\frac{\partial G^{\pm}}{\partial L}=\mp\frac{\partial L}{\partial Ud}\frac{\partial G^{\pm}}{\partial\epsilon}, \quad \text{(C19)}$$

$$\frac{\partial G^{\pm}}{\partial\theta}=-\sin\theta\frac{\partial L}{\partial\cos\theta}\frac{\partial G^{\pm}}{\partial L}$$

$$=\pm\sin\theta\frac{\partial L}{\partial\cos\theta}\frac{\partial G^{\pm}}{\partial\epsilon}. \quad \text{(C20)}$$

The other partial derivatives of E involving $\mathbf{q}$ can also be evaluated in a similar way.

APPENDIX D. TRANSVERSE CONTRIBUTION NEAR SADDLE POINTS

The integral to be evaluated (60) can be written as the principal part of

$$A_0{}^{\mathrm{sp}}(q)=(2q)^{-1}\int_{-b}^{+b}\frac{S(\mu-z^2)}{z+\frac{1}{2}q}\,dz, \quad \text{(D1)}$$

where μ is measured from ϵ_{sp}, b depends on μ, and the chosen region R, and $S(\mu-z^2)$ is the cross-sectional area of the Fermi surface at z, and in R

$$S(E)=\int^{x,y\epsilon R}dx\,dy\theta(x^2+y^2-E). \quad \text{(D2)}$$

It is convenient to choose a cubic region of integration R such that

$$-a\leq z\leq a,$$

$$-a\leq\tfrac{1}{2}\sqrt{2}(\pm x\pm y)\leq a, \quad \text{(D3)}$$

one then has

$$S(E)=2a^2[1+(E/a^2)(1-\ln\mid E/a^2\mid)], \quad \text{(D4)}$$

and

$$b=(a^2+\mu)^{1/2};\qquad \mu<0,$$

$$b=a;\qquad \mu\geq 0. \quad \text{(D5)}$$

This should be substituted in (D1). As a function of z the cross-sectional area $S(\mu-z^2)$ is a symmetrical function with maximum at $z=0$. Its most important feature is the logarithmical divergence of the derivative which appears for

$$z/a=\pm\alpha, \quad \text{(D6)}$$

when

$$\mu/a^2=\alpha^2>0. \quad \text{(D7)}$$

The behavior of the integral (D1) depends on the position of the singularity at $z=-\frac{1}{2}q$ in relation to these points.

It can be shown that $A_0{}^{\mathrm{sp}}(q)$ [Eq. (D1)] is finite for all q.

The integral (D1) can be decomposed into several parts. The only part which can show a singular behavior when

$$q=2\alpha a \quad \text{(D8)}$$

is

$$A_2(\alpha,\gamma)=\frac{\alpha}{4\gamma}(1-\gamma^2)\int_0^{1/\alpha}\frac{\ln\mid 1-x\mid}{x-\gamma}\,dx, \quad \text{(D9)}$$

where

$$x=z/\alpha a;\qquad \gamma=q/2\alpha a. \quad \text{(D10)}$$

This integral vanishes for

$$\gamma=1, \tag{D11}$$

and is obviously finite with well-defined derivatives anywhere else. Separating regions of integration:

$$A_2(\alpha,\gamma)=\bar{A}_2(\alpha,\gamma)+\frac{2\alpha a}{4\gamma}(1-\gamma^2)$$
$$\times\left[\int_0^{1-\epsilon} dx\,\frac{\ln|1-x|}{x-\gamma}+\int_{1+\epsilon}^{\alpha} dx\,\frac{\ln|1-x|}{x-\gamma}\right], \tag{D12}$$

where

$$\bar{A}_2(\alpha,\gamma)=\frac{2\alpha a}{4\gamma}(1-\gamma^2)\int_{1-\epsilon}^{1+\epsilon} dx\,\frac{\ln|1-x|}{x-\gamma}, \tag{D13}$$

and ϵ is small but assumed large compared to $|1-\gamma|$.

The discontinuity is obviously in $\bar{A}_2$. Now

$$\bar{A}_2(\alpha,\gamma)=\frac{2\alpha a}{4\gamma}(1-\gamma^2)$$
$$\times\left[\ln|1-\gamma|\ln\left|\frac{1-\gamma+\epsilon}{1-\gamma-\epsilon}\right|+\int_{-\epsilon/1-\gamma}^{\epsilon/1-\gamma} du\,\frac{\ln|u|}{1-u}\right], \tag{D14}$$

where

$$u=(1-x)/(x-\gamma). \tag{D15}$$

We are interested in the derivatives with respect to γ (i.e., q) in the limits

$$\gamma\to 1^+$$

and

$$\gamma\to 1^-.$$

It can be seen that

$$\lim_{\gamma\to 1}\frac{d}{d\gamma}\left[\frac{(1-\gamma^2)}{\gamma}\ln\left|\frac{1-\gamma+\epsilon}{1-\gamma-\epsilon}\right|\ln|1-\gamma|\right]=0, \tag{D16}$$

because

$$\ln\left|\frac{1-\gamma+\epsilon}{1-\gamma-\epsilon}\right|\sim 2\left(\frac{1-\gamma}{\epsilon}\right) \tag{D17}$$

for small $1-\gamma$, and

$$\lim_{\gamma\to 1}(d/d\gamma)[(1-\gamma)^2\ln|1-\gamma|]=0. \tag{D18}$$

We are thus left with

$$\tilde{A}_2(\alpha,\gamma)=-\frac{\alpha a}{\gamma}(1-\gamma^2)\int_0^{\epsilon/1-\gamma} du\,\frac{\ln|u|}{u^2-1}. \tag{D19}$$

Now,

$$\frac{d\tilde{A}_2(\alpha,\gamma)}{dq}=\frac{1}{2\alpha a}\frac{d\tilde{A}_2(\alpha,\gamma)}{d\gamma}$$
$$=-\frac{\tilde{A}_2}{2\gamma}-\epsilon\frac{(1-\gamma^2)}{\gamma}\frac{\ln\epsilon-\ln|1-\gamma|}{\epsilon^2-(1-\gamma)}+\tfrac{1}{2}I(\gamma), \tag{D20}$$

where

$$I(\gamma)=\int^{\epsilon/(1-\gamma)} du\,\ln|u|/(u^2-1). \tag{D21}$$

In the limit $\gamma\to 1$, the two first terms on the right side of (D20) vanish. For the last term we have the discontinuity

$$I^-=\lim_{\gamma\to 1-} I(\gamma)=\int_0^{\infty} du\,\frac{\ln|u|}{u^2-1}=+\tfrac{1}{4}\pi^2, \tag{D22}$$

$$I^+=\lim_{\gamma\to 1+} I(\gamma)=\int_0^{\infty} du\,\frac{\ln|u|}{u^2-1}=-\tfrac{1}{4}\pi^2, \tag{D23}$$

and therefore the discontinuity in the derivative is

$$\Delta dA/dq\,|_{\gamma=1}=\lim_{\gamma\to 1-}(dA/dq)-\lim_{\gamma\to 1+}(dA/dq)=\tfrac{1}{4}\pi^2. \tag{D24}$$

We have thus shown that the derivative of $A^{sp}(q)$ has a discontinuity when (D8) holds.

It is interesting to note that the discontinuity is a local effect of the sp and its size does not depend on the size of the region of integration. As a result, a discontinuity in the derivative of this magnitude will appear even when the effect of the sp is only felt in a very small part of the Fermi surface.

Figure 2 shows the results of a numerical evaluation of the integral (D1) for three values of μ. It can be seen that for $\mu>0$ the derivative is positive and increasing for small q and decreases discontinuously at the point (D8).